PNL-3948
UC-70

Fracturing of Simulated High-Level Waste Glass in Canisters

R. D. Peters
S. C. Slate

September 1981

Prepared for the U.S. Department of Energy
under Contract DE-AC06-76RLO 1830

Pacific Northwest Laboratory
Operated for the U.S. Department of Energy
by Battelle Memorial Institute

Battelle

PNL-3948

PACIFIC NORTHWEST LABORATORY
operated by
BATTELLE
for the
UNITED STATES DEPARTMENT OF ENERGY
Under Contract DE-AC06-76RLO 1830

Printed in the United States of America
Available from
National Technical Information Service
United States Department of Commerce
5285 Port Royal Road
Springfield, Virginia 22151

Price: Printed Copy $_____*; Microfiche $3.00

*Pages	NTIS Selling Price
001-025	$4.00
026-050	$4.50
051-075	$5.25
076-100	$6.00
101-125	$6.50
126-150	$7.25
151-175	$8.00
176-200	$9.00
201-225	$9.25
226-250	$9.50
251-275	$10.75
276-300	$11.00

PNL-3948
UC-70

FRACTURING OF SIMULATED HIGH-LEVEL WASTE GLASS IN CANISTERS

R. D. Peters
S. C. Slate

September 1981

Prepared for
the U.S. Department of Energy
under Contract DE-AC06-76RLO 1830

Pacific Northwest Laboratory
Richland, Washington 99352

ACKNOWLEDGMENTS

The authors are grateful to numerous contributors. M. L. Longaker and D. P. Williams provided experimental assistance. D. P. Williams also assisted in data analysis. F. A. Simonen and R. J. Shippell provided Appendix A on fracture modeling. L. R. Bunnell provided the section on particle size analysis. Editing by G. B. Long was valuable in the writing and organization of the report.

SUMMARY

Waste-glass castings generated from engineering-scale developmental processes at the Pacific Northwest Laboratory are generally found to have significant levels of cracks. This report discusses the causes and extent of fracturing in full-scale canisters of waste glass as a result of cooling and accidental impact. The work was performed at the Pacific Northwest Laboratory under the High-Level Waste Container Development Project, part of the U.S. Department of Energy's Long-Term High-Level Waste Technology Program technically coordinated by Savannah River Laboratory. Although the effects of cracking on waste-form performance in a repository are not well understood, cracks in waste forms can potentially increase leaching surface area. If cracks are minimized or absent in the waste-glass canisters, the potential for radionuclide release from the canister package can be reduced. Additional work on the effects of cracks on leaching of glass is needed. In addition to investigating the extent of fracturing of glass in waste-glass canisters, methods to reduce cracking by controlling cooling conditions were explored.

In this report, thermal fracturing is studied in canisters of glass produced by continuous melting and in-can melting. Although both processes have been considered for the solidification of nuclear wastes, the continuous-melting process is currently receiving much interest in the United States. Thus, continuous melting-produced canisters are emphasized here.

The extent of fracturing in continuous-melting-produced canisters cooled at different rates and using fixed amounts of insulation without auxiliary heating or cooling (called "passive cooling") is discussed. Results show that the ratio of crack surface area to the surface area of a monolithic cylinder is 18 for continuous melting-produced canisters cooled in about 50 hours from peak glass temperatures (about 850^{o}C). Surface area increases by a factor of 7 for a canister cooled in 100 hours. In addition, fracturing in a canister with internal carbon-steel fins is examined. Although fins increase heat transfer, thus lessening thermal gradients in the glass, the extent of

cracking is not significantly reduced because of the difference in glass and metal fin thermal expansion rates.

Since accidental impacts can occur during handling or transportation of canisters, surface area measurements (from particle size analyses) were taken of cracked glass in two dropped in-can-melting-produced canisters. These measurements were compared to the analysis of glass from a nonimpacted in-can-melting canister. Canisters 40 cm and 30 cm in dia were dropped from 9- and 30-m heights, respectively. The glass in both canisters had roughly 7 times the surface area of that of the nonimpacted canister.

Experiments were also performed on scaled-down canisters to study effects of casting and cooling techniques on cracking. A 17-cm-dia canister was filled from a laboratory-scale melter and cooled such that the glass was nearly crack-free. Extrapolation of the cooling time from this size to full scale indicates that 18 to 20 days of cooling would be required to form a crack-free 60-cm-dia waste-glass casting.

It was found that when bench-scale canisters were cooled in three stages, cooling time could be shortened over "passive" times without increasing fracture damage. This was accomplished by first rapid-cooling during filling, which quickly brought down glass temperatures. Next, large radial gradients were reduced by slow cooling immediately after filling. Finally, rapid cooling was employed to bring the glass to handling temperatures.

Overall, the study shows that the extent of glass cracking in full-scale, passively-cooled, continuous melting-produced canisters is strongly dependent on the cooling rate. This observation agrees with results of previously reported Pacific Northwest Laboratory experiments on bench-scale annealed canisters. Thus, the cause of cracking is principally bulk thermal stresses. Fracture damage resulting from shearing at the glass/metal interface also contributes to cracking, more so in stainless steel canisters than in carbon steel canisters. This effect can be reduced or eliminated with a graphite coating applied to the inside of the canister.

Thermal fracturing can be controlled by using a fixed amount of insulation for filling and cooling of canisters. In order to maintain production rates, a

small amount of additional facility space is needed to accomodate slow-cooling canisters. Alternatively, faster cooling can be achieved using the multi-staged approach. Additional development is needed before this approach can be used on full-scale (60-cm) canisters.

CONTENTS

FIGURES

INTRODUCTION

Large-scale waste-glass castings are susceptible to significant fracturing as experience has shown at engineering-scale process development facilities. In this document, the cause and extent of fracturing are reported for canisters of glass produced from continuous melting (CM), and to a lesser extent, for glass produced from in-can melting (ICM). In the CM process, canisters are filled with molten glass produced in a continuously operating furnace. The ICM process is a batch operation in which waste glass is formed in the canister with externally supplied heat. Both processes have been considered as a means of solidifying wastes although the CM process is currently receiving the most interest. This report focuses on thermal fracturing; however, impact fracture data that accompany the accidental drop of an ICM canister are presented. Fracturing in dropped CM canisters has been described previously by Bunnell (1978).

Although specific criteria pertaining to cast-glass integrity have not been established, it is desirable to produce a casting with as few cracks as practical. Relative to highly fractured castings, waste glass with few or no cracks has low surface area to allow leaching of radionuclides. However, cracked surface area is not necessarily as readily available for leaching as an open-glass surface. Perez and Westsik (1980) found leaching from cracks after 40 days to be one-third to one-half as fast as leaching from open-glass faces. Below certain crack widths, no leaching was observed, although large uncertainties were reported in their data. Although compressive forces of the canister wall tend to keep glass fragments in place, if and when a canister fails, significant crack separations may develop. Ethridge, Clark, and Hench (1979) discuss the deleterious effects of water trapped for days between separated glass and note pH excursions and increased glass corrosion rates. Absence of cracks, or few cracks, may simplify and improve confidence in leaching calculations used for repository analysis. Requirements for high-integrity barriers may be lessened if cracks in the waste glass are reduced.

The benefits of few or no cracks in a glass-filled canister must be weighed against added costs resulting from the complexities in the

vitrification plant that will be incurred during production of these canisters. The effect of different process options on degree of fracture is explored in this report, and this information may be useful in a cost-benefit analysis.

The first section of the report discusses full-scale (60-cm-dia) waste-glass canisters. The effects of cooling are examined by analyzing temperature gradients and radial cross-sections of the canisters. Also, impact fracture is examined in 30- and 40-cm-dia ICM canisters via particle size analysis. In addition, the relative importance of bulk thermal stresses and metal canister-imposed stresses is discussed. Modeling of glass/canister interaction, described in Appendix A, is useful in providing a perspective on thermal- versus canister-imposed stresses.

The second section describes experiments that used bench-scale (17-cm-dia) canisters, which are relatively inexpensive and convenient to perform. In this section, different cooling methods and canister designs are investigated.

CONCLUSIONS

In this work, the causes and extent of fracturing in waste-glass have been investigated. The principal findings of this report are summarized below:

- Bulk thermal stresses are the predominant cause of fracturing in glass poured by continuous melting into insulated canisters where glass/metal bonding is not extensive.
- Some damage occurs at the glass/metal interface as a result of thermal expansion differences and is more severe in stainless steel canisters than carbon steel canisters. This damage can be reduced by preventing bonding and reducing friction using a graphite coating on the inside of the canister.
- The surface area increase due to fracturing was determined by examining cross sections that were obtained by slicing full-scale (60-cm-dia) CM glass castings. A cooling period of 100 hours resulted in an increase of surface area over exterior canister area by a factor of 7, and cooling for 50 h resulted in an increase of 18. This cooldown time applies to a passive, single-stage condition where a fixed amount of insulation is used for filling and cooling.(a)
- Thermal gradients in glass can be diminished while glass is still above its softening point (550°C) by cooling in three stages. This method was found to significantly speed cooling over single-stage cooling without significantly increasing the level of cracks.
- Carbon-steel fins that fill 5% of the internal volume reduce thermal gradients but, due to thermal expansion mismatch between the glass and metal, do not reduce cracking significantly.

(a) Previous work has shown that the cooling of canisters without insulation takes about 25 h and results in an increase in surface area of 27.

- Drop-test results show that fracture surface area increased by less than an order of magnitude when ICM canisters were dropped from 9- and 30-m heights.

Thermal fracturing can be controlled by applying insulation to the canister during filling and cooling. A projected cooldown period of about 20 days is needed in order to completely eliminate thermal cracks. Fairly low levels of fracturing will result from a 4-day cooldown (factor of seven increase as mentioned above). Space requirements to hold canisters for 4 days should not be very significant in a processing plant although this judgement will depend on specific processing details. To decrease this space by speeding cooling without increasing cracks, more complicated schemes are required such as the multistaged cooling method described above. The full impact of cooling methods on a waste solidification process needs to be addressed before specific cooling procedures can be recommended.

FRACTURING IN FULL-SCALE CANISTERS

Thermal fracturing in continuous melting-produced (CM) canisters of glass is discussed in this section through an examination of crack patterns in glass and their comparison with the thermal history of the glass. Fracturing of glass in an in-can-melter (ICM) canister is discussed, although only qualitatively in comparison with the CM canisters (the thermal history of the ICM canister is not discussed). Additionally, impact fracture damage to two ICM canisters is examined using the technique of Bunnell (1978). Samples of cross-sectioned canisters are analyzed to determine the cause of fracturing (drop-tested canisters were not cross-sectioned).

The glass compositions of cross-sectioned specimens are Savannah River simulated waste compositions, similar to either TDS-211 or TDS-131 as described by Dierks et al. (1980). The CM canisters were fabricated from carbon steel and have a 60-cm OD and a 0.64-cm-thick wall. Internally located thermocouples provide temperature profiles and history. The thermally fractured ICM canister has a 60-cm OD x 1.6-cm-thick wall and is made from 304L stainless steel. The impact-fractured canisters are 30- and 40-cm OD x 0.64-cm-thick wall and were filled with PW-7 waste glass.

The principal method of canister examination was to saw radial cross-sections with commercial concrete-cutting equipment. A subcontractor performed canister sectioning with 90-cm-dia diamond-impregnated blades. Figure 1 illustrates the arrangement for cutting the 60-cm-dia canisters (a 40-cm-dia canister is being cut here). To reduce blade wear, a 2.5-cm-wide metal strip around the canister perimeter at the cut location was removed via air-arc torch.

CONTINUOUS-MELTING CANISTERS

A fairly wide range of cooling conditions is represented by the four CM canisters (see Table 1 for canister process information). During filling and cooling, canisters were placed in an enclosure insulated with 8 cm of ceramic fiber insulation (conductivity = 5×10^{-4} W/cm-^{o}K). The enclosure was

DOE-Richland, WA

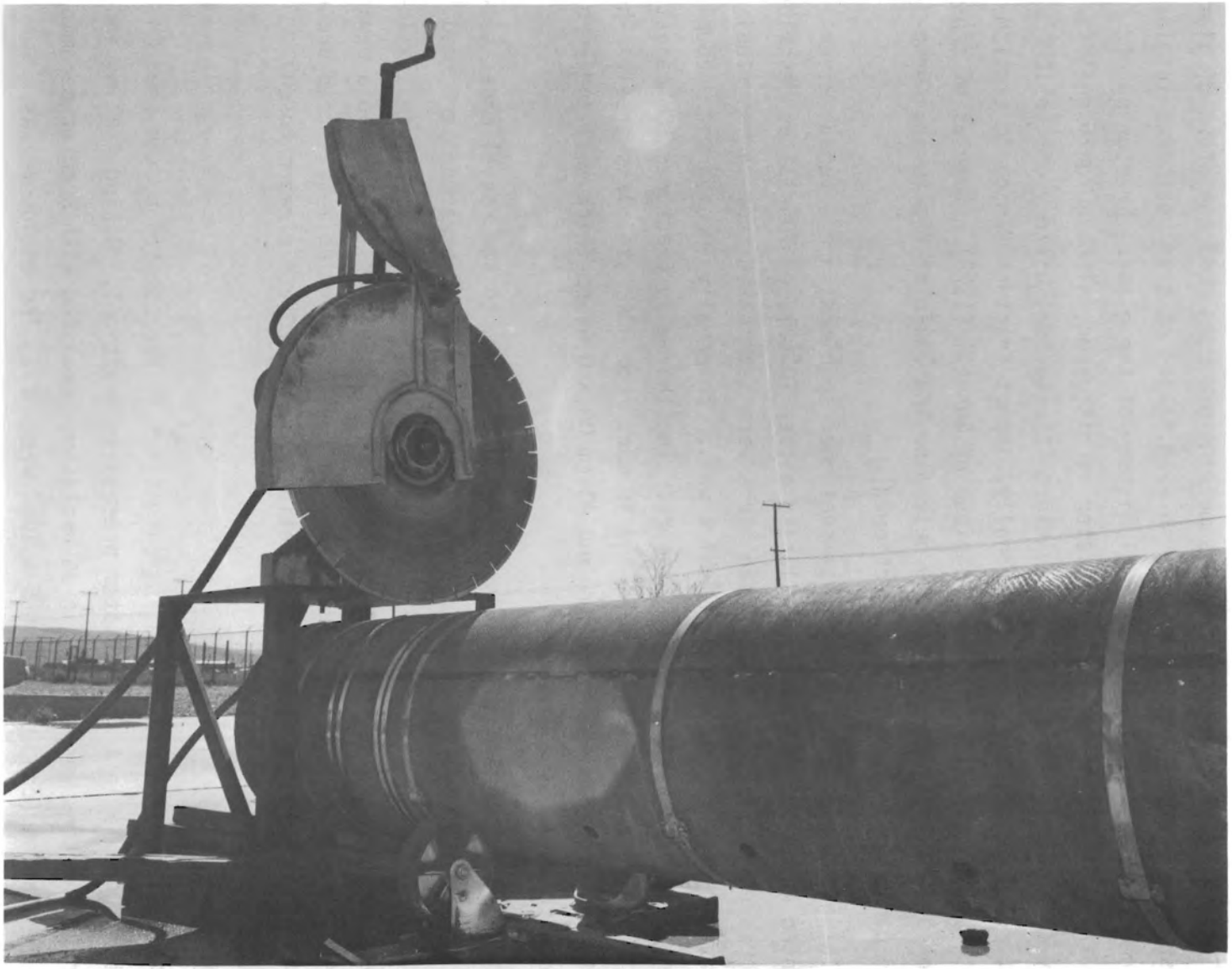

FIGURE 1. Radial Cross-Sectioning Arrangement for Full-Scale Canisters

TABLE 1. Glass-Filled Canister Process Information[a]

Canister Number	Date Filled	Fill Rate, kg/h	Length, cm	Weight (Canister + Glass), kg	Melter[b] Used	Comments	Average Centerline Cooling Rate, °C/h
144	5/5/81	50	290	1300	LFCM	Slow cooled in double enclosure	8
150	7/14/79	60	290	2110	LFCM	10 internal fins, forced-air cooled	20
151	1/15/81	100	290	1750	LFCM	Cooled in single enclosure	14
200	6/11/79	56	240	1760	CFCM	Forced-air cooled after filling	15

(a) All canister casings are of carbon steel, 60 cm dia with 0.64-cm-thick walls.
(b) LFCM--Liquid-Fed Ceramic Melter; CFCM--Calcine-Fed Ceramic Melter.

designed to hold up to a 90-cm-dia canister so that an 15-cm-wide annulus existed between a 60-cm canister and the enclosure inside wall. This large annulus provided a significant pathway for heat loss to the environment. The double enclosure indicated for CM Canister 144 was 2.5-cm-thick insulation wrapped tightly around the canister before the canister was placed in the enclosure. Forced-air cooling was accomplished by passing room temperature air through the annulus at ∿300 CFM, or at a velocity of about 400 cm/s.

Canister 150 was constructed with 10 internal carbon-steel fins (0.64 cm thick) that extended 2 cm from the wall to 8 cm from the center. These fins were equally spaced (36^{o} apart) and ran the length of the canister. Internal fins were originally developed for heat transfer during processing and storage of waste canisters with high thermal loads. In this case, fins were used to reduce temperature gradients during filling. Stainless steel fins were found to cause significant fracture damage in 20-cm-dia canisters as a result of the large thermal expansion mismatch between stainless steel and waste glass (Simonen and Slate 1979).

Centerline temperatures during filling and cooling of CM canisters are shown in Figure 2 for individual mid-axis locations. These temperature transients are average for the canister. Due to the time it takes to fill canisters with glass, the top of the canister is, in terms of the progress of

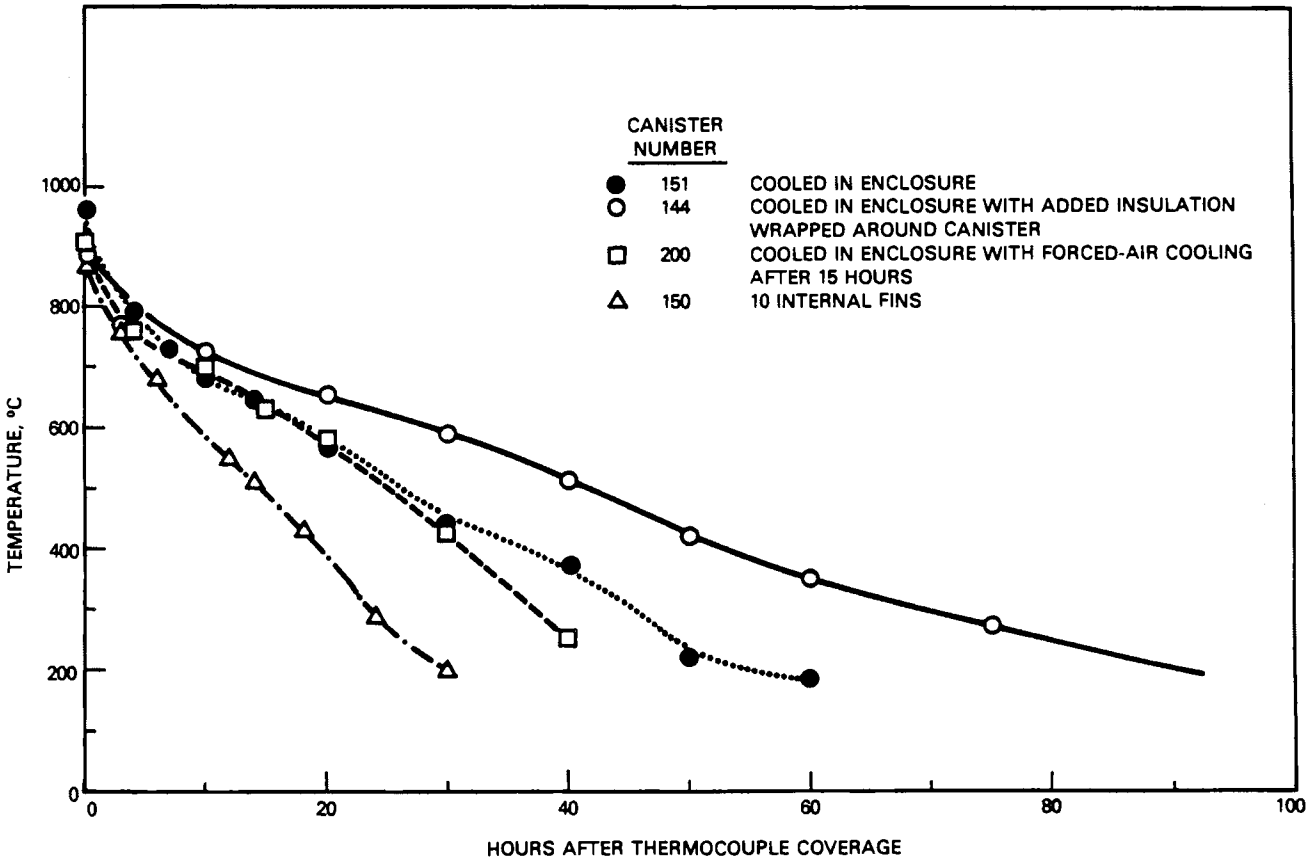

FIGURE 2. Centerline Temperatures of 60-cm-dia Canisters Filled from Continuous Melters

cooling, 10 to 15 h behind the bottom of the canister. Zero on the time scale refers to the instant that molten glass, upon entering the canister, covered internal thermocouples. A major part of cooldown occurs during the filling stage. Internal fins in CM Canister 150 increased the cooling rate substantially, as Figure 2 shows. In the absence of fins, cooldown times ranged from 50 to 90 h.

Figure 3 shows the crack pattern representative of glass cooled at relatively fast rates in a CM canister. The cooling history and temperature profiles are given in Figures 2 and 4. Axial gradients in full-scale canisters are generally 1.5 to 2.5°C/cm, whereas radial gradients are typically greater than 20°C/cm in the outer radial positions. During cooling of Canister 200

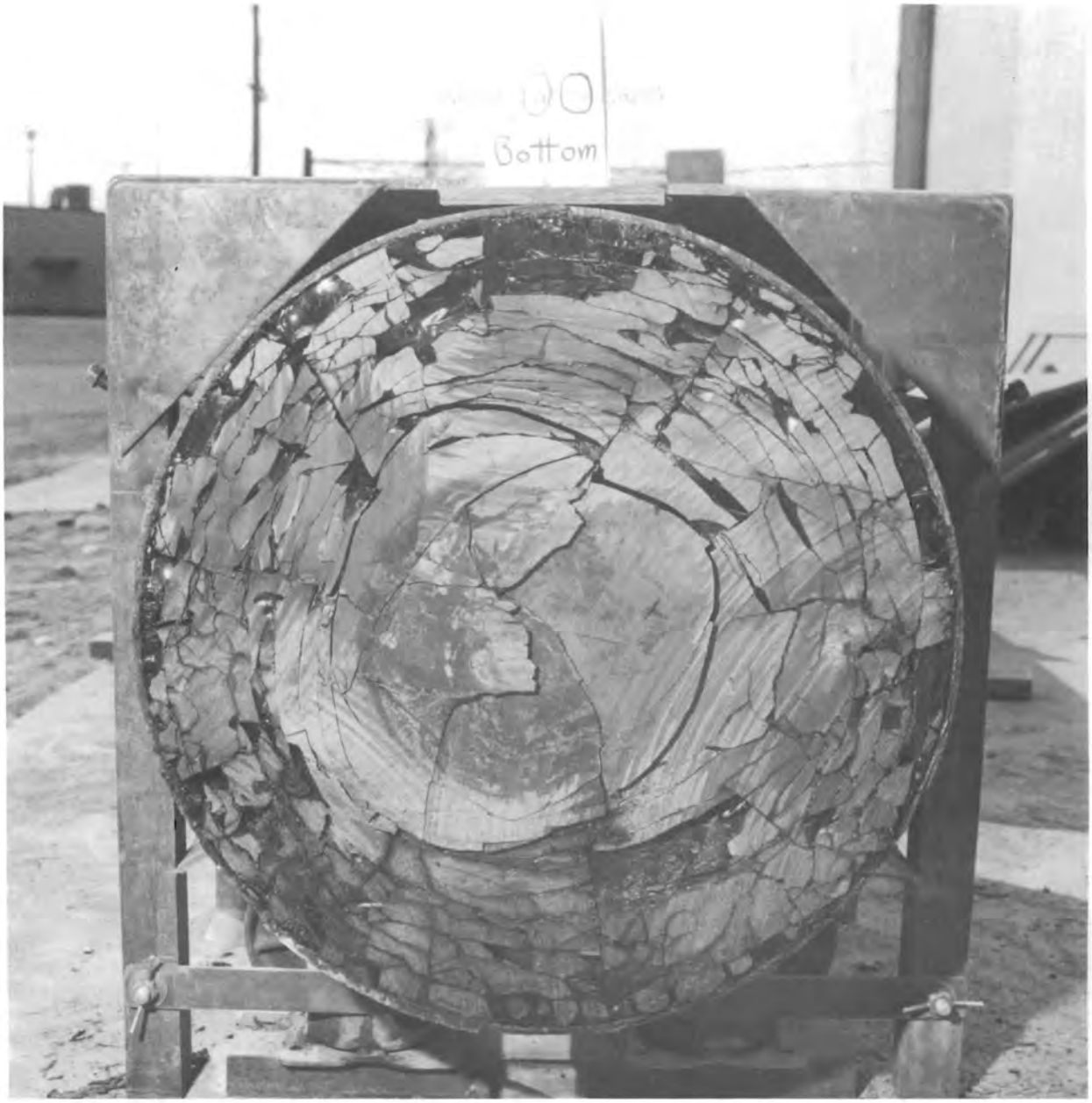

FIGURE 3. Sixty-Centimeter-Diameter Cross Section of Canister 200, 100 cm from Bottom

in the first 15 h (Figure 2), slight natural convection occurred since small ports at the bottom of the enclosure were open to air; after 15 h, forced air was used. Sharp gradients developed compared to those of Canister 144, which was well insulated. Glass fragments resulting from fracturing are roughly

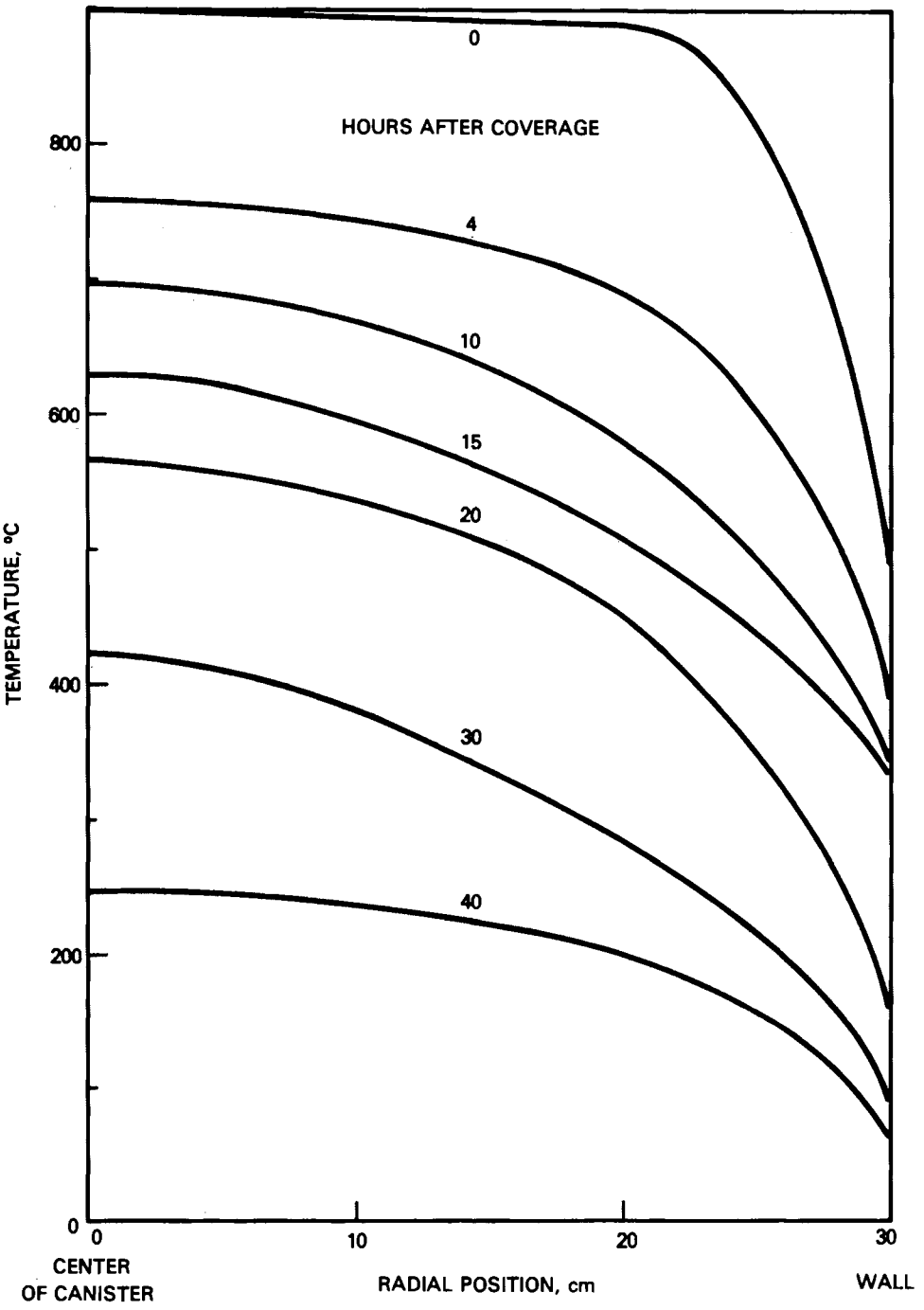

FIGURE 4. Radial Temperature Profiles for Canister 200, Forced-Air Cooled After 15 h

constant in size from about mid-radius to the wall, with perhaps smaller fragments within 1.3 to 2.5 cm from the wall. These fragments are 1.5 to 2.5 cm in size; many have 5- to 8-cm-long axes oriented concentrically. A small amount of the fracture damage near the wall can be attributed to thermal shock from air-arc torch removal of a strip of the canister before sawing. Inwards from mid-radius, larger fragments are encountered, and the center region of the canister (about 1/3 of the radius) consists of several very large, 8- to 16-cm-size fragments. As Figure 4 shows, temperature gradients determined for the outer radius are quite high between 4 to 10 h after the thermocouples were covered, and range from 20 to 40^{o}C/cm. These gradients exist while the glass is undergoing transition from the soft or molten state (about 550^{o}C) to the brittle state.

When the glass finally cools, reverse strain develops (Slate et al. 1978; Pincus and Holmes 1977), which is relieved by glass fracture. A series of radial cracks spaced every 30 to 40^{o} apart and extending from about mid-radius to the wall is evident in Figure 3. These cracks are probably the result of hoop stresses.

The radial cross-section and temperature profiles for Canister 151 are not shown since they resemble those of Canister 200. The same insulation as in Canister 200 was used in Canister 151; no forced-air cooling was used.

Figure 5 shows the result of fairly slow cooling (Canister 144). Temperature gradients are greatly reduced when the canister is wrapped with 2.5-cm insulation, in addition to being placed in the enclosure as seen in Figure 6. The damage is much reduced compared to that of Canister 200 (Figure 3), which was cooled about twice as fast. The cross section in Figure 5 is characterized by large fragments that have edges of 10 to 20 cm. Glass fragments 5 to 15 cm in size fell away from this cross-section plane, leaving depressions. Fracturing is generally more severe near the wall, but in a few locations a large fragment borders with the metal canister. The slow cooling apparently caused some crystallization in the glass since brown discoloration is visible, especially near the wall. Crystals evidently nucleated on the iron oxide coating of the carbon steel canister. Westsik et al. (1979) have shown that devitrification has a minimal effect on glass leaching.

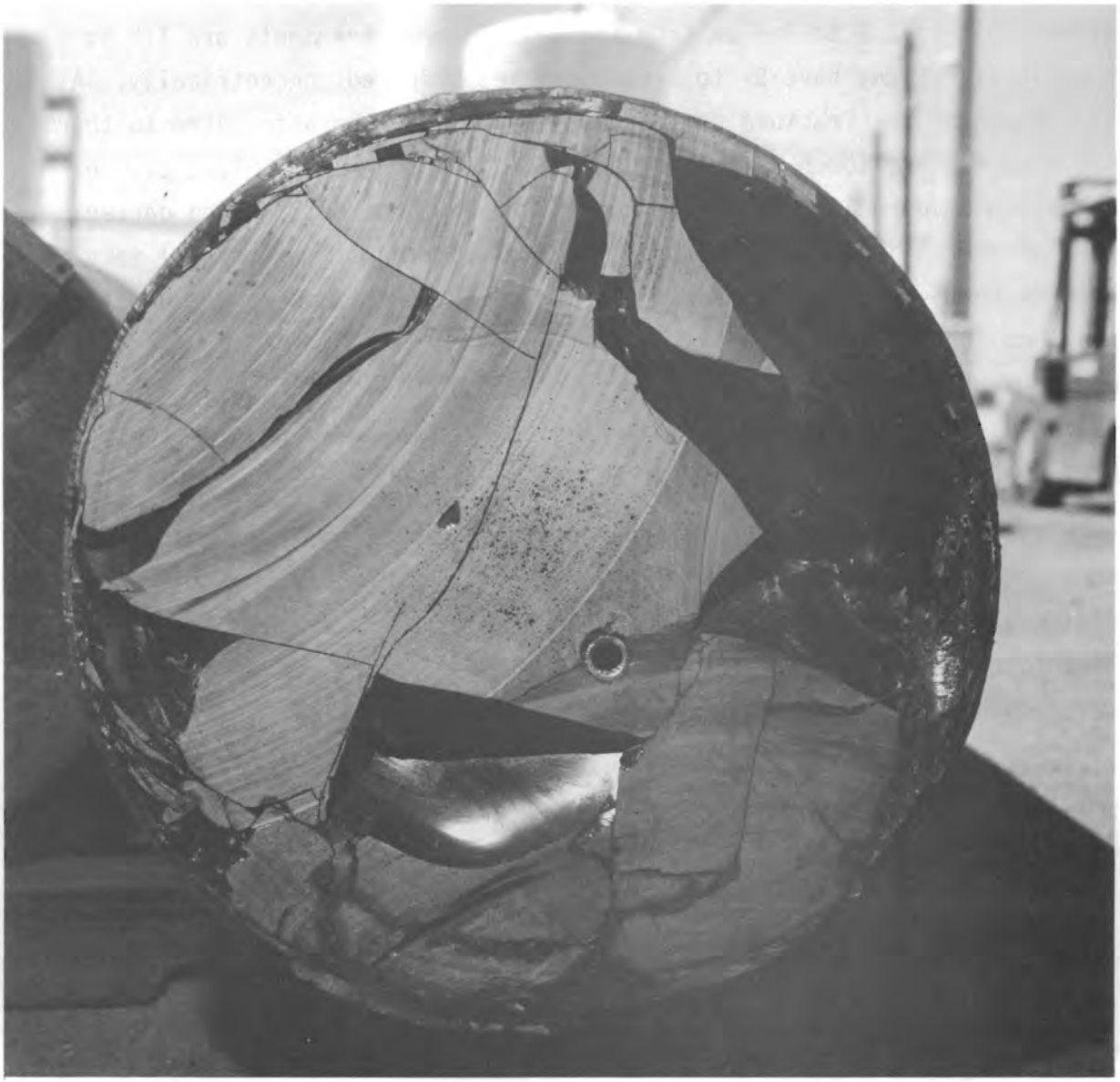

FIGURE 5. Sixty-Centimeter-Diameter Cross Section of Canister 144, 60 cm from Bottom

Because of difficulties encountered when sawing through steel fins, only a partial cross section is available for finned Canister 150 (see Figure 7). The use of internal carbon-steel fins was effective in reducing gradients in Canister 150, as Figure 8 shows. Gradients near the wall were steep because

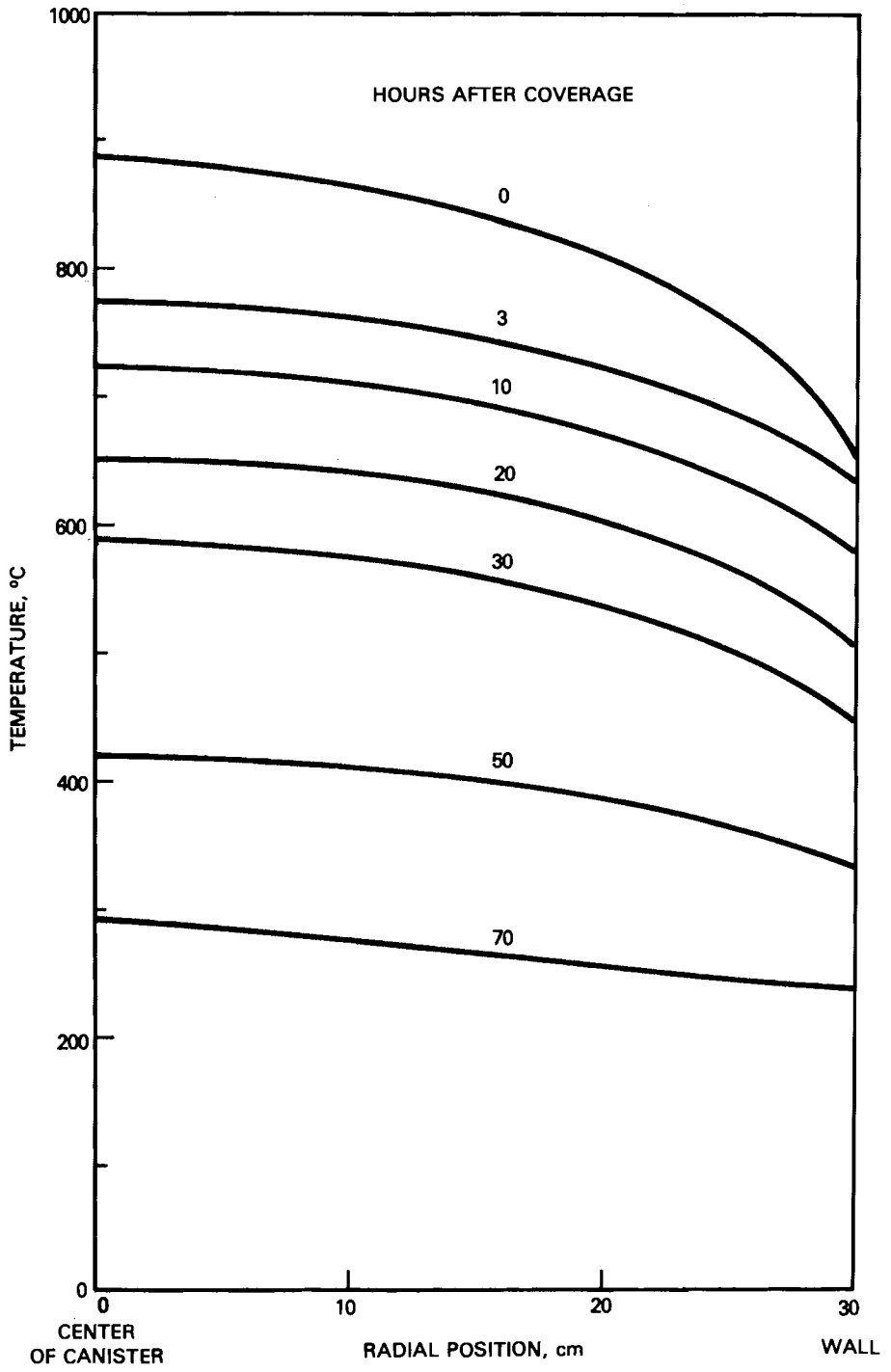

FIGURE 6. Profiles for Canister 144, Filled and Slow Cooled With Same Insulation

FIGURE 7. Partial Section of Canister 150 (60 cm dia) with Ten Internal Fins, 130 cm from Bottom

the fins extended only up to about 2.5 cm from the wall as Figure 7 shows. Profiles through the bulk of the radius are quite similar to those of Canister 144, which took 90 h to cool (the finned canister only took 35 h to cool).

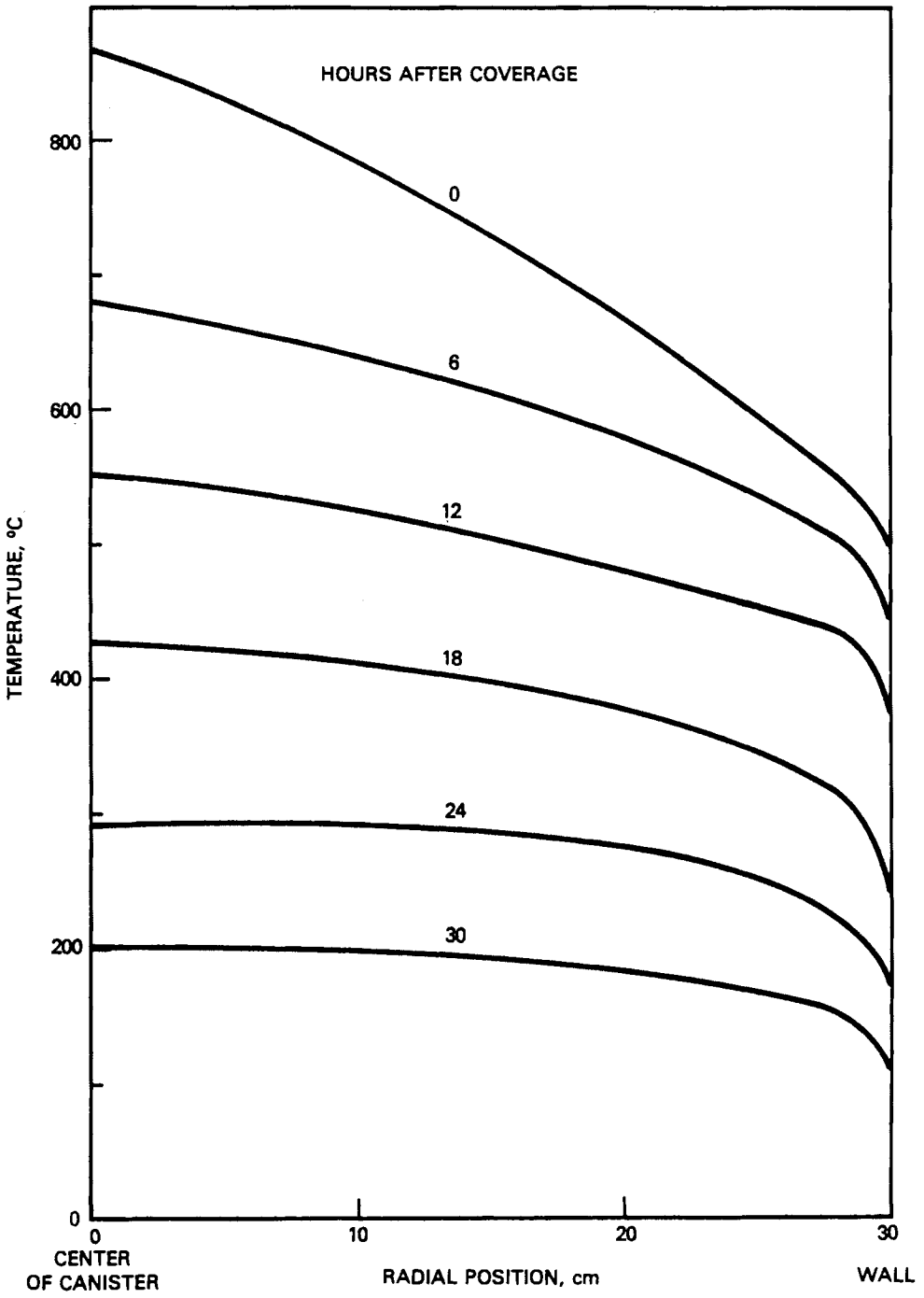

FIGURE 8. Profiles for Canister 150 Having 10 Internal Fins

Fracturing in this canister is fundamentally different than that in canisters without fins. Cracks seem much more randomly oriented compared to cracks in the cross-section in Figures 3 or 5. More fracturing occurs near

the outside wall, which can be largely attributed to a fairly sharp temperature drop through this region (see Figure 8). The gradients 5 to 8 cm from the wall are fairly flat and are similar to gradients found 5 to 10 cm from the center of Canister 200, as Figure 4 shows. However, the fracturing is much more extensive at this wall location in Canister 150 that at the center of Canister 200. Thus, in addition to thermal stresses, interaction between carbon steel and glass, which have different thermal expansion coefficients, probably accounts for fracturing. Cracks run parallel to the fins, particularly to the middle fin in Figure 7, which may have been caused by shearing of the glass. Glass is well bonded to the fins, as the right side of the figure shows. Here an exposed fin is covered with adhered glass. A major difference between this radial section and those of canisters without fins is the tight compression of fragments that occurs in this canister. Sawing did not vibrate any fragments and widen the cracks as occurred in the canisters without fins. Also few, if any, fragments could be extracted from the cross-section, whereas in other canisters many fragments tended to fall out. Apparently, fins compress against the glass and offer structural support.

SURFACE AREA MEASUREMENTS FOR CM CANISTERS VERSUS COOLING TIME

In this section, a quantitative measure of the increase in geometric surface area resulting from glass fracture is reported. Surface area is measured from cross sections of canisters that were cooled in 100 h (Canister 144), 55 h (Canister 151), and 45 h (Canister 200). Surface area for Canister 150 with fins was not determined. Cracks, which appear as line segments in the cross-section photographs, are added up and then divided by the superficial area of a cylinder (per unit length; ends are neglected), $2\pi r$, to give a relative area increase. Fines are not accounted for but are minimal in these canisters. In practice, several representative wedges of about 25^{o} are measured. The surface area increase of a single axial location is extrapolated for the entire canister. This approximation is reasonable since most of the canister experiences a similar thermal gradient history. This technique is subject to errors due to the resolution of the photographs and approximations made in measuring crack lengths. Based on repeated measurements, surface areas are estimated to be ±25% of reported values.

For the fast-cooled Canisters 200 and 151, the estimated relative surface areas are 17 and 18; for the slower-cooled Canister 144, a value of 7 is found. A CM canister filled and cooled without insulation cools down in about 25 h (Chapman et al. 1979). Slate et al. (1978) measured the surface area of such a canister by excavating out fragments and performing a particle-size analysis. At the glass-metal interface, they found extensive fracturing; for the whole canister, a relative increase of about 27 was obtained. Much of this damage is attributed to thermal shock of hot glass contacting cool metal, which generated fine particles. Due to those fines, about 1 wt% of the glass contributed to 50% of the surface area. Without fines, the relative surface area would be about 14. These data are plotted in Figure 9 as a function of cooldown time. Considering the uncertainty shown in Figure 9, there is no significant difference between the surface area for Canister 151, Canister 200 and Slate's measurement without fines. A straight, flat line has therefore been drawn between these data. The point at 450 h represents a crack-free glass monolith; the cooling time required is estimated based on experiments with 17-cm-dia canisters.

Figure 9 can be used as a "trade-off" curve when considering the practicalities of a production facility and the desire to reduce cracks. The disadvantage of long cooling times is that additional space is needed to hold cooling canisters before subsequent handling. Fines represent a small percentage of the inventory and may be considered unimportant. If this is the case, then in terms of bulk cracks, the no-insulation case can be grouped with canisters that have been moderately insulated (see the solid line, Figure 9) and there is thus, no incentive for moderate insulation. There is a greater advantage, however, in going to 100 h of cooling, but beyond this the curve flattens out again.

The impact of prolonged cooling on processing depends upon details of post-fill canister-handling procedures and facilities. It is beyond the scope of this document to discuss the details of various handling options and their costs. However, it is worth noting the minimum space requirements for cooling over long periods. The number of canisters undergoing cooldown is the cooldown

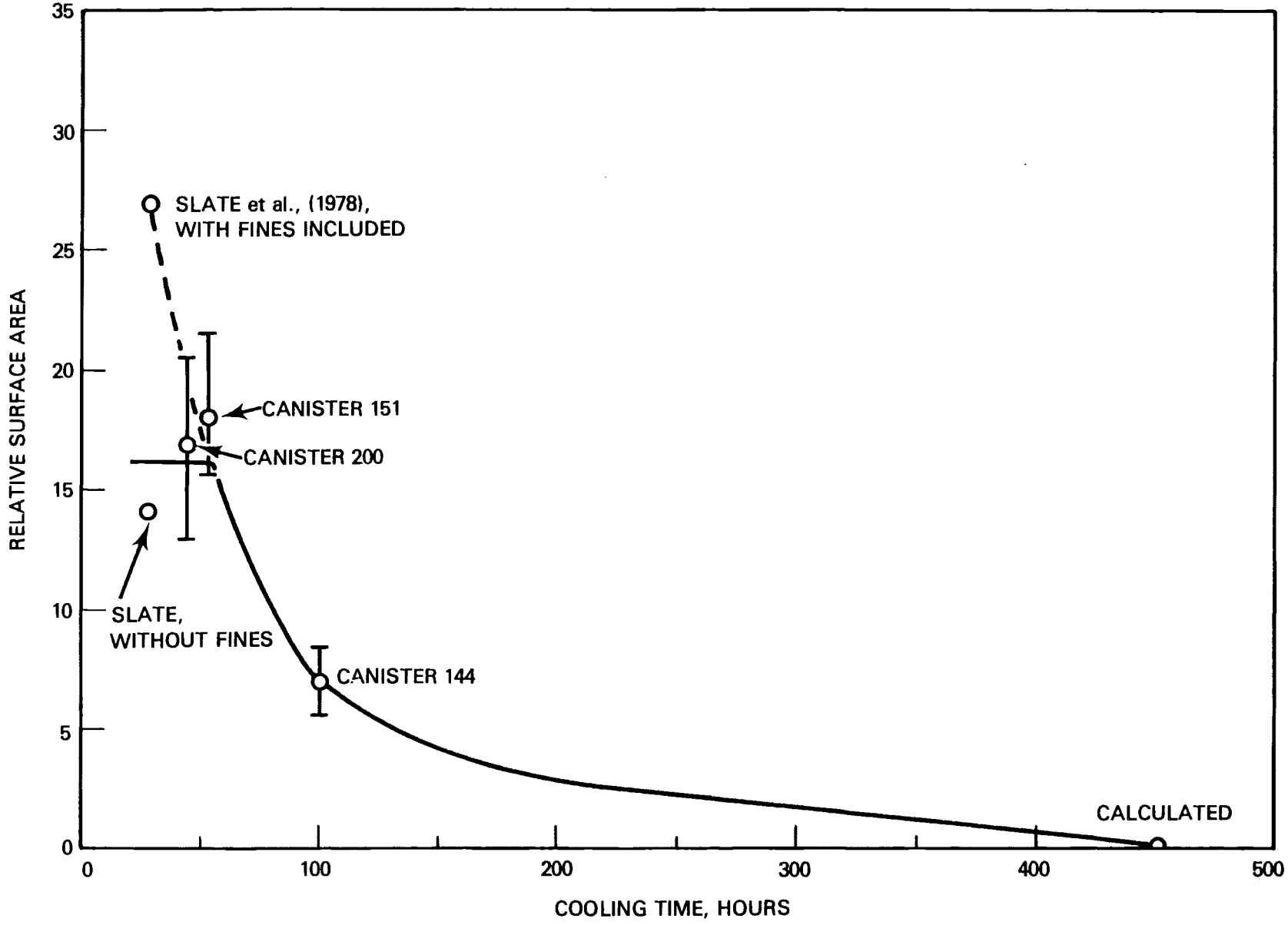

FIGURE 9. Effect of Cooling Time on Relative Surface Area of Thermal Cracks in Glass Cast in 60-cm-dia Carbon Steel Canisters

time multiplied by the production rate. The Savannah River Laboratory reference CM process calls for 1 to 1.5 canisters per day. Thus, for a 100-h cooldown, as in Canister 144 discussed above, 4 to 6 canisters at any given time would be cooling down. Leaving room for insulation and cooling air, this would require about 4 to 6 m^2 of floor space. This is about 5% of the mechanical cell space in the preliminary design of the Savannah River Defense Waste Processing Facility.

IN-CAN-MELTING CANISTER

The radial cross-section of Canister ICM-7, produced at the Savannah River Laboratory (SRL) TNX development facility, is shown in Figure 10. During inspection, many loose fragments fell away, but enough of the cross-section remains intact to permit characterization. Some similarities are evident between this canister and Canister 200 (Figure 3). The center is essentially intact, and similar to Canister 200, concentrically oriented fragments prevail from about mid-radius to the wall. Within about the last inch up to the canister wall, fracturing becomes rather extensive, and cracks are less than 0.32 cm apart. This type of fracture is inherently different than the type found in the CM canisters where much larger fragments are observed. It is likely that the thermal expansion mismatch between the stainless steel and glass caused shear stresses and thus fractured the glass. During cooldown, shear forces due to resistance to movement of the canister relative to the glass are determined by their difference in thermal expansion coefficient. This difference is 8.2 x $10^{-6}/^{o}C$ between 304L stainless steel and TDS-411, whereas for carbon steel, the difference is only 3.1 x $10^{-6}/^{o}C$. Also, stainless steel bonds to glass much more aggressively than does carbon steel, probably due to the absence of a thick oxide layer on stainless steel. Futhermore, ICM canisters are subjected to higher temperatures (1050 to 1100^{o}C) than CM cans, which increases enameling of glass to the canister wall.

SIZING OF GLASS IN AS-FILLED AND DROP-TESTED ICM CANISTERS

Drop or collision impact of a waste-glass canister is a possible accident during handling and transportation. This is a continuation of impact testing

FIGURE 10. Partial Section of Canister ICM-7 (60 cm dia), 60 cm from Bottom

done previously at PNL by several investigators. In 1977, Slate (see Simonen and Slate 1979) performed extensive impact testing of metal-canister integrity but did not report the extent of glass damage. Bunnell (1978) evaluated the fracturing of several CM cans dropped by Slate using particle-size analysis.

Smith and Ross (1975) studied fractured glass in impacted annealed 17-cm-dia dropped canisters. In this section, results of drop tests performed by Slate in 1977 on commercial full-scale (30- and 40-cm-dia) ICM canisters are reported. Particle-size analyses are performed on glass from two dropped canisters and are compared to the analysis of an ICM canister that was not dropped but which underwent similar processing thermal history.

Sieve sizing was performed on glass-fragment samples from three ICM canisters of simulated nuclear waste glass. The three canisters are briefly characterized as follows:

- Canister 39--As-filled; not drop tested; 30 cm OD; 304L SST canister
- Canister 45--Drop-tested; 30 m height; 40 cm OD; 304L SST canister
- Canister 8--Drop-tested; 9 m height; 30 cm OD; 304L SST canister.

Sampling was done by the judicious use of hammers and screwdrivers to pry fragments out of place with minimal force to avoid generating more fines. The outer 2.5 cm of glass nearest the canister wall were sampled separately from the rest of the glass in order to note any size differences. Coarse sieving was done using an orbital shaker and large (20-cm-dia) screens. For sieve sizes finer than 0.85 mm, a sonic sifter was used. A 30-min shake time was used for coarse particles (1 h for fines). A plot was constructed of cumulative weight percent finer than a given sieve size for each canister, and are included as Figures 11 through 13. The results were first plotted on log-normal paper after the work of Mecham, Jardine, Pelto and Steindler (1980), since this method produces an easily extrapolatable line. In this case, however, a straight line did not result, which indicated that the size distribution did not follow the statistical normal curve. In the two test cases used, more fine particles were evident than in a normal distribution. As a result, the data are plotted on log-log paper simply as a convenient way to show all data.

When comparing the glass sizes of the two dropped canisters with that of the as-filled canister, the effect of impact testing is obvious. Originally, the mass-median particle size in the as-filled canister was about 27.6 mm, including one suspect data point. If this point is ignored, the median size is 22.6 mm. Both of the dropped canisters have median sizes close to this

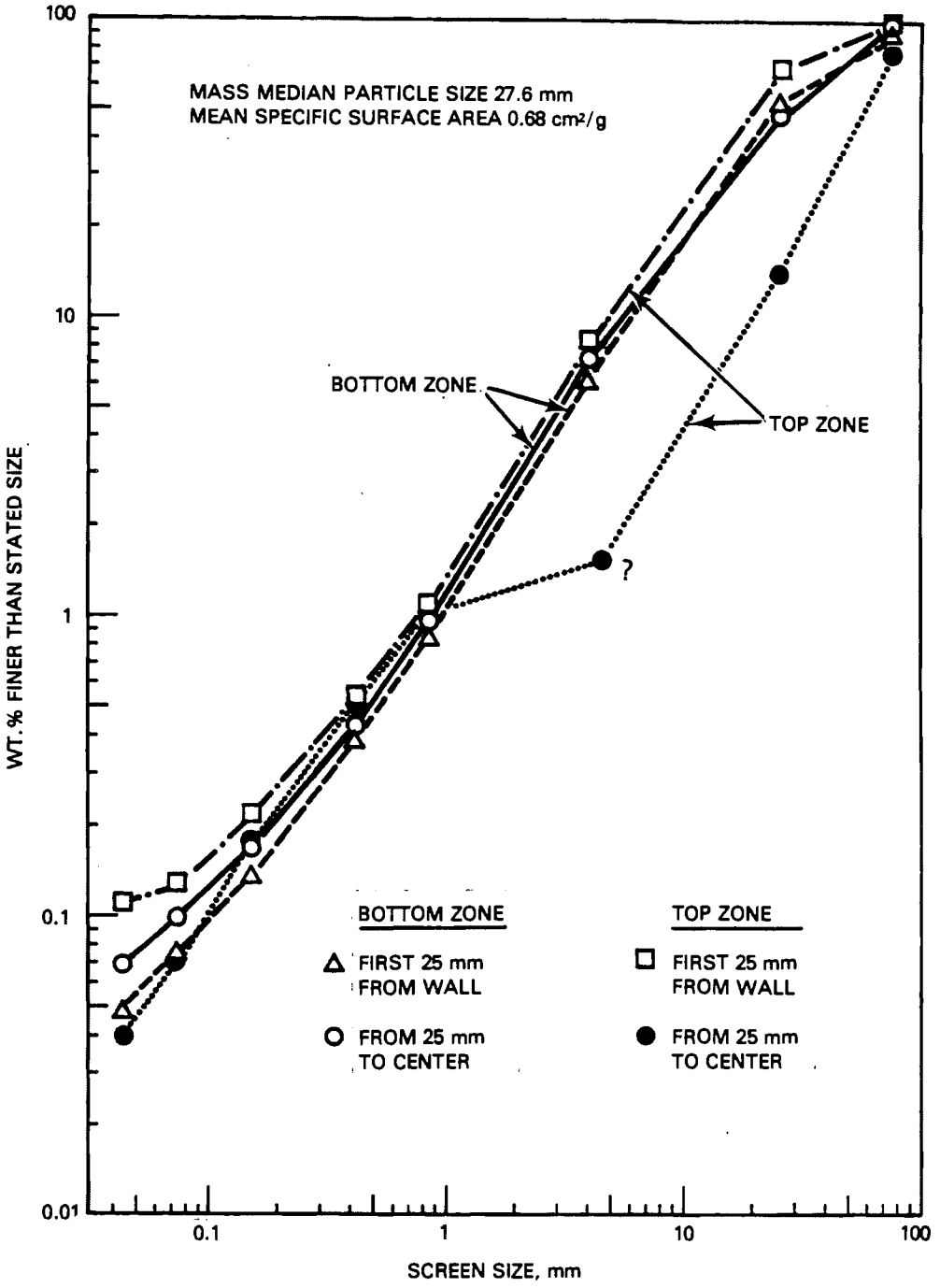

FIGURE 11. Particle-Size Distribution for Various Axial Positions in 30-cm-dia ICM (Not Drop-Tested) Canister

value at the upper region of the canister, which is virtually unaffected by impact--17.8 mm for Canister 45 and 21.5 mm for Canister 8. In contrast, impact testing produced a grossly different size distribution in the heavily

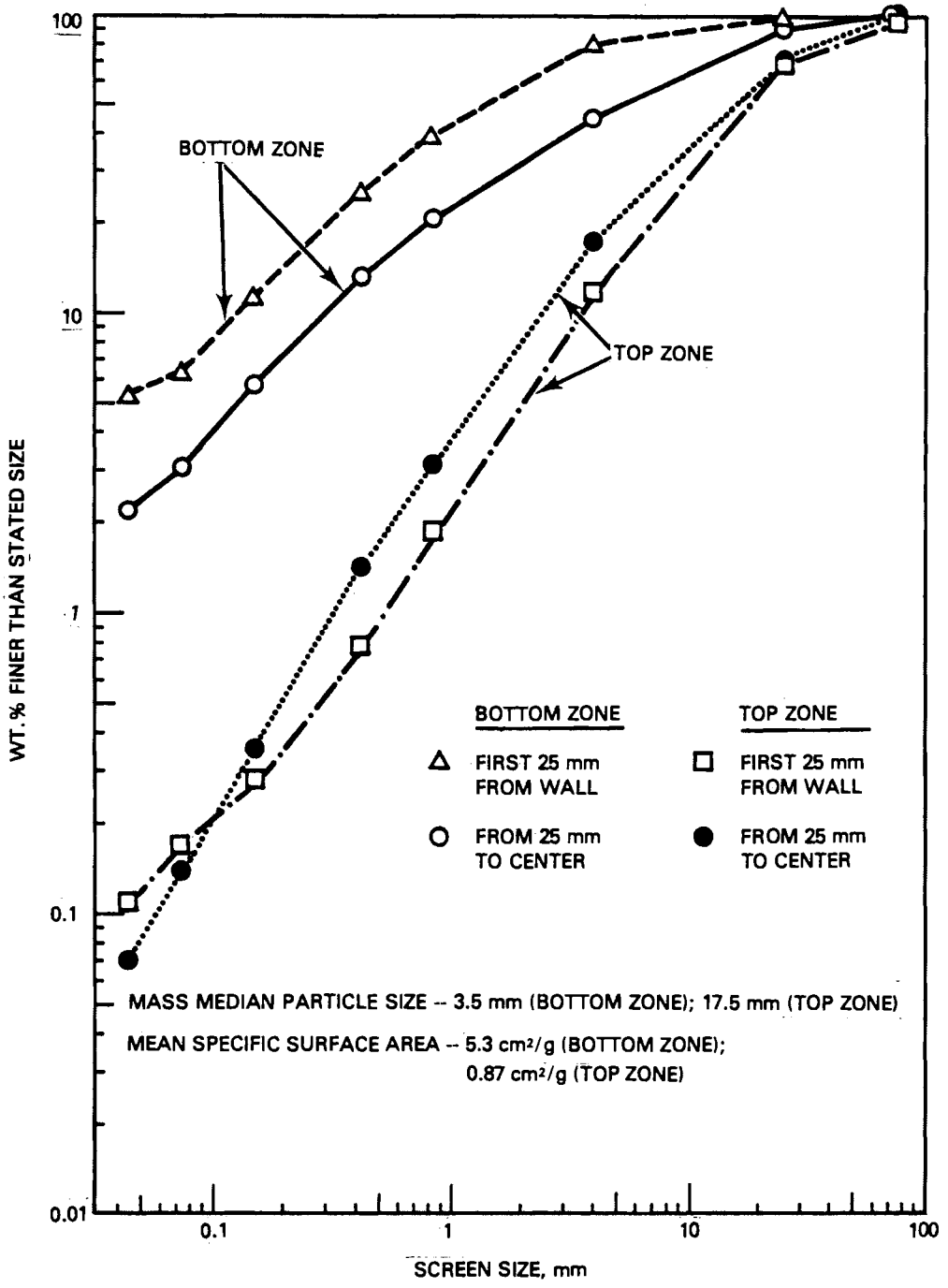

FIGURE 12. Particle Size Distribution for Various Axial Positions in 40-cm-dia Canister Dropped from 30-m Height

damaged zone, which is estimated at not more than about 0.7 m in height. The glass in the heavily damaged region had a mass median size of 3.0 mm (Canister 8) and 3.5 mm (Canister 45). Note that the greater impact energy and velocity

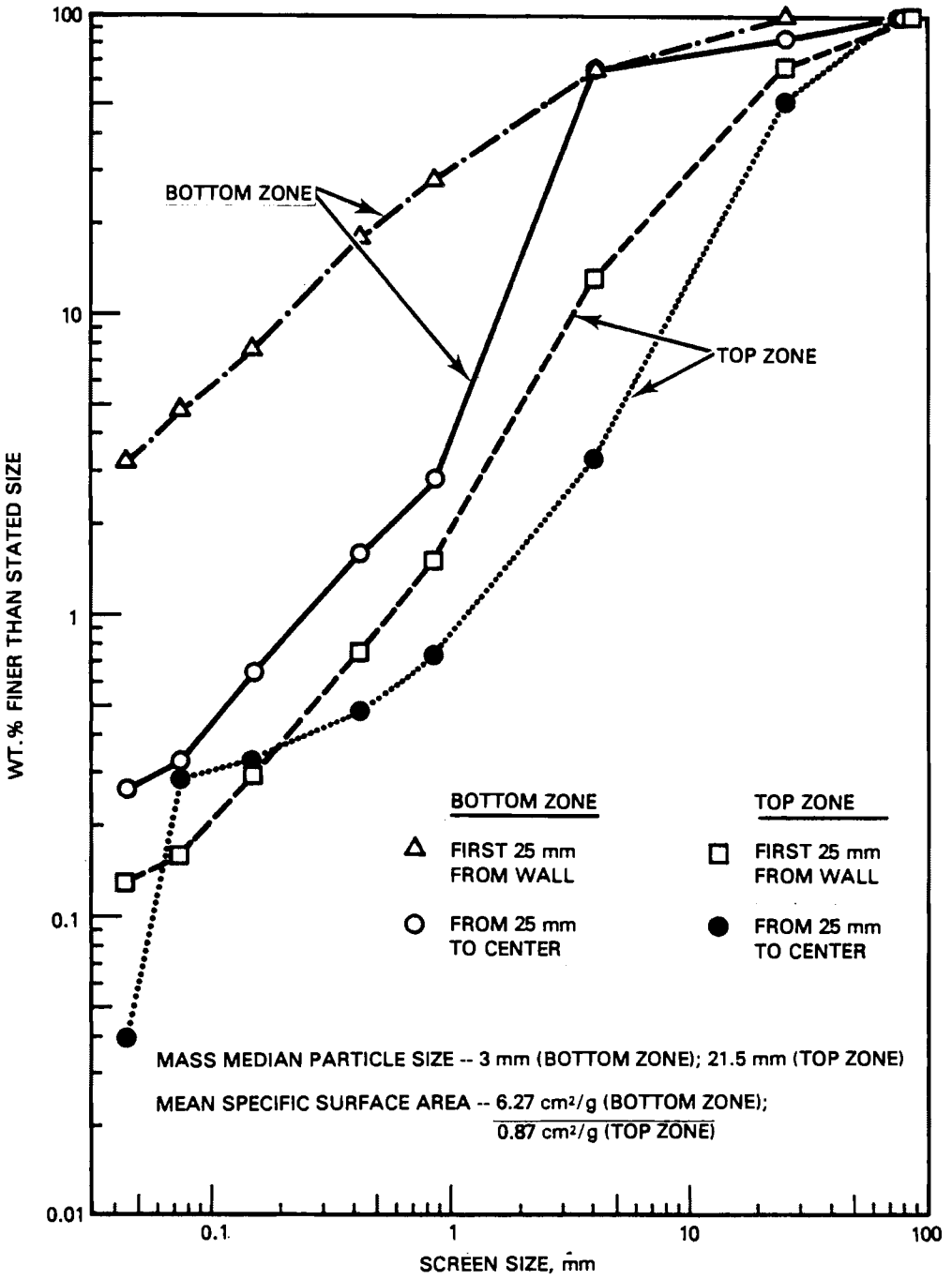

FIGURE 13. Particle Size Distribution for Various Axial Positions in 30-cm-dia Canister Dropped from 9-m Height

of the higher-dropped canisters have made little if any difference in the size distribution, as if a saturation effect had limited the production of more fines in a single impact. Because of the difference in size and weight of the two canisters, it is probably a mistake to make detailed comparisons.

When sampling at two radial locations, it was noted that little size difference was evident between inner and outer glass (see Figure 11). Using screen sizing and the density of the glass in the canisters ($\sim$3.2 g/cm^3), and assuming spherical particles, some rough geometric surface areas can be calculated. The numbers are shown on the appropriate figures and vary from 0.68 cm^2/g for the as-filled canister to 6.27 cm^2/g for the impacted glass.

CAUSE OF FRACTURE

The cause of cracking in waste-glass-filled canisters has been discussed by Slate et al. (1978). Fracturing results from either thermal gradients or the bonding coupled with thermal expansion mismatch at the glass/metal interface. In thermal fracturing, the extent of cracking increases with the magnitude of the temperature gradients. This relationship is clearly evident when comparing the gradients of Canisters 200 and 144 (Figures 4 and 6) with their cross sections (Figures 3 and 5). These gradients are established during casting when glass is "soft" (nonbrittle). When glass finally cools, reverse strain develops (Pincus and Holmes 1977), which leads to fracturing. The dependence of cracking level on cooling rate was shown in Figure 9.

At shorter cooling times than used for Canisters 151 and 200 (see Figure 9), as with Slate's data without fines, the bulk-glass fracturing does not increase. Evidently a limiting cooling rate has been achieved. It is possible that glass fractures into minimum-sized fragments at these higher cooling rates due to the distribution of weaknesses in the casting. Owing to their small size, these fragments may be impervious to the higher cooling rates possible under these processing conditions.

If glass/canister interaction were the dominant cause of fracture damage, then the extent of cracking would be largely independent of cooling rate (and thus temperature gradients). In Appendix A, cracks resulting from glass/canister shear stresses are modeled. The conclusion is that the glass/metal thermal expansion mismatch will result in damage over a region no more than the wall thickness of the canister. This type of damage is not seen in the cross sections of CM canisters (carbon steel), but is observed in the ICM canister (stainless steel), which was cross-sectioned.

Thus, thermal stresses are the most important cause of fracture in CM canisters made of carbon steel. Stainless-steel CM canisters could potentially develop glass/metal shear fracture. This could be reduced if a coating, such as the graphite tested in a small-scale canister, was used. In ICM canisters, both shear and thermal stress are important. The shear fracture is confined to about the outer 2 cm of the glass.

In the drop-tested ICM canisters, most of the impact damage was confined to the bottom portion of the canisters where impact occurred. The top zones were nearly unaffected; most of the fracturing in this region was due to thermal gradients from the cooldown.

It is doubtful that the effects of sawing action cause much of the evident fracturing. First, the crack patterns at the cutting interface resemble those observed 8 to 10 cm underneath the cutting interface when a section of fragments is lifted out. It is not likely that fracturing caused by the sawing would propagate this far and result in similar crack patterns. Second, the distribution of cracks through the canister radius is what could be expected based on the nature of the cooling process. The sawing action does, however, tend to increase crack widths because of mechanical vibration of glass fragments.

BENCH-SCALE EXPERIMENTS ON GLASS COOLING AND CRACKING

A series of tests on a bench scale (17-cm-dia canisters) was performed in order to conveniently examine how different casting and cooling methods affect glass cracking. The primary objective of these tests was to gain a qualitative understanding of the effects of cooling rate on various canister designs and on graphite coating used on the inside wall of metal canisters. Smith and Wiley (1981) at SRL have investigated the effects of various liners and cooling rates on 5-cm-dia castings produced by in-can melting. Higher glass temperatures in this process aggravate both the glass/metal bonding problems and the thermal gradients upon cooldown. Ross (1975) studied cooling of 17-cm-dia canisters but used an in-can melting-casting method. The continuous melting casting used in this study more closely resembles a full-scale continuous melting process.

Glass-filled canisters were cast from an existing PNL one-third-scale joule-heated melter. The normal filling rate was 30 kg/h. Canisters were made from 17-cm-dia pipe (0.34-cm-thick wall), either carbon steel or 304L stainless steel. Thin-walled canisters were also used (0.16-cm-thick wall). The 80-cm-long canisters were open at the filling end. A cooldown receptacle was designed to apply varying degrees of insulation.

In this study, the effects of cooling rate were experimentally determined by measuring the extent of cracking from cross sections as done for full-scale canisters. These experiments also provide an estimate of glass strength. A cooling procedure that involves three stages is then discussed. Finally, damage due to glass/metal interaction is discussed.

EFFECTS OF COOLING RATE

The effects on cracking of cooling at different rates can be seen in the first three cross sections of Figure 14A-D.

Canister 1 (Figure 14A) was filled and cooled with 5 cm of ceramic fiber insulation (conductivity, 5×10^{-4} W/cm^{o}K) around the cooling pod. The centerline temperture was 100^{o}C after 40 h. This was the slowest cooldown performed during the bench-scale tests. Except for some gouges caused by

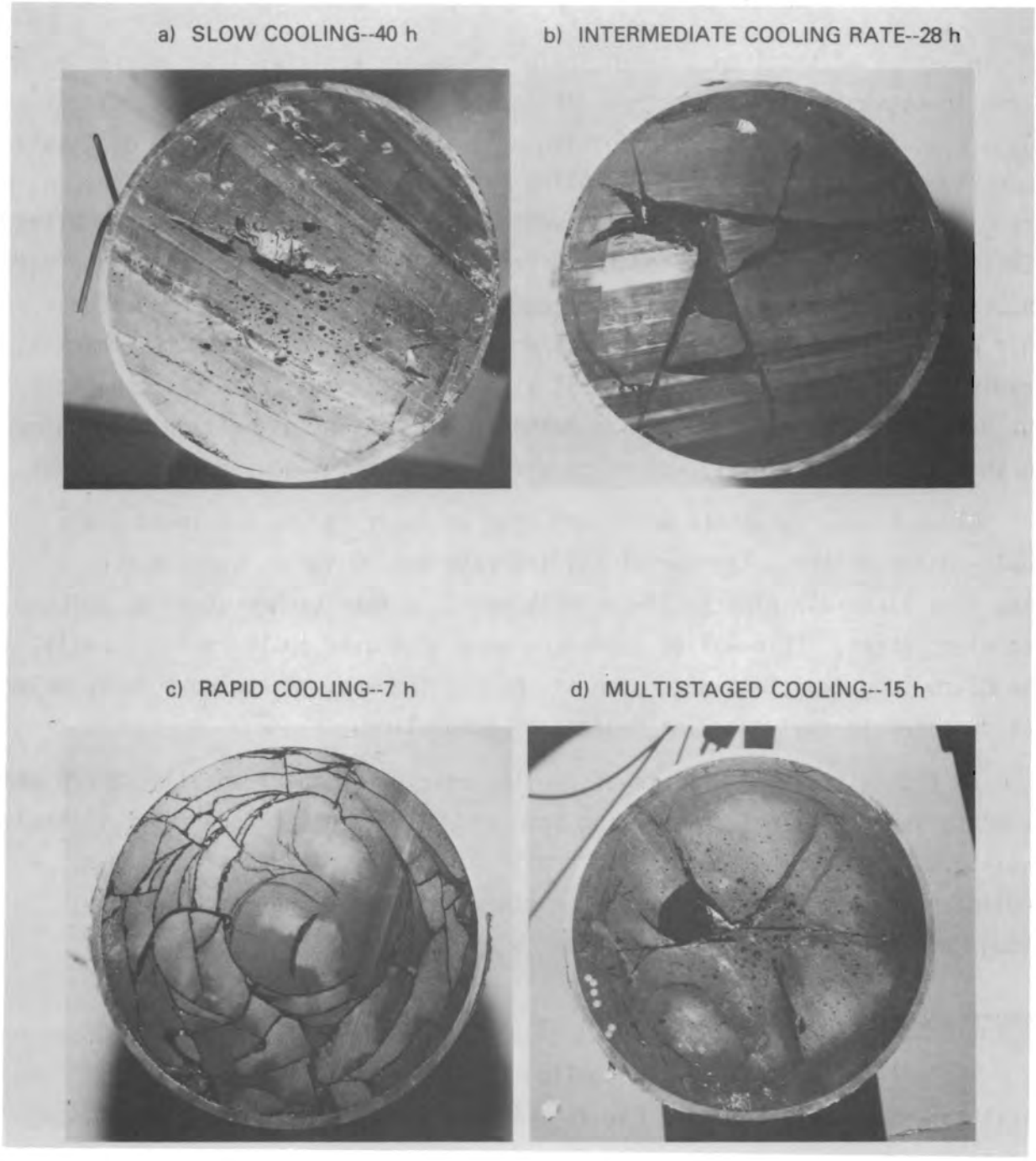

FIGURE 14A-D. Cross Sections of Bench-Scale, 17-cm-dia Canisters

aggressive cutting, the cross section of this canister is nearly crack-free. Canister 2 (Figure 14B) cooled in 28 h with 2.5 cm of kaowool insulation and was clearly damaged from cracks.

A rapid cooldown was accomplished for Canister 3 (Figure 14C), which was filled and cooled without insulation. The centerline was initially 850°C and the wall only 450°C. The centerline reached 100°C after 6.5 to 7 h. Extensive fracturing occurred as Figure 14C shows. The crack pattern in this cross section has many of the features seen in full-scale Canister 200 (Figure 3). Concentric cracks prevail at outer radii, and the center is relatively crack free.

The relative surface area increase for these canisters is plotted on logarithmic coordinates as a function of cooldown time in Figure 15. Shown for comparison is the full-scale canister curve which is somewhat parallel to the bench-scale data. The bench-scale data includes a point by Ross (1975). Surface area reported by Ross was obtained by particle-size analysis; however, in this study crack lines from cross sections were measured. Evidently the two methods give similar results. The bench-scale curve begins to slope downward at longer cooling times.

The thermal history of these tests can be used with stress analysis to estimate the tensile strength of the waste glass. The maximum centerline-to-wall temperature drop for Canister 2 was about 140°C; for Canister 1 this drop was about 70°C. Thermocouples along the radius of 1 show that a parabolic temperature profile is established within minutes after the thermocouples are covered with glass. For an initial parabolic profile, the residual hoop stress σ_θ is proportional to the maximum centerline-to-wall temperature difference ΔT as shown in Appendix B:

$$\sigma_\theta = \frac{1}{2} \frac{\alpha E \Delta T}{(1-\nu)} \qquad (1)$$

where α is thermal expansion of glass ($9 \times 10^{-6}/^{\circ}C$); E is Young's modulus (7.6×10^4 MPa); and ν is Poisson's ratio (0.3). The strength of the glass in Canister 1 was not exceeded significantly during cooldown, whereas in

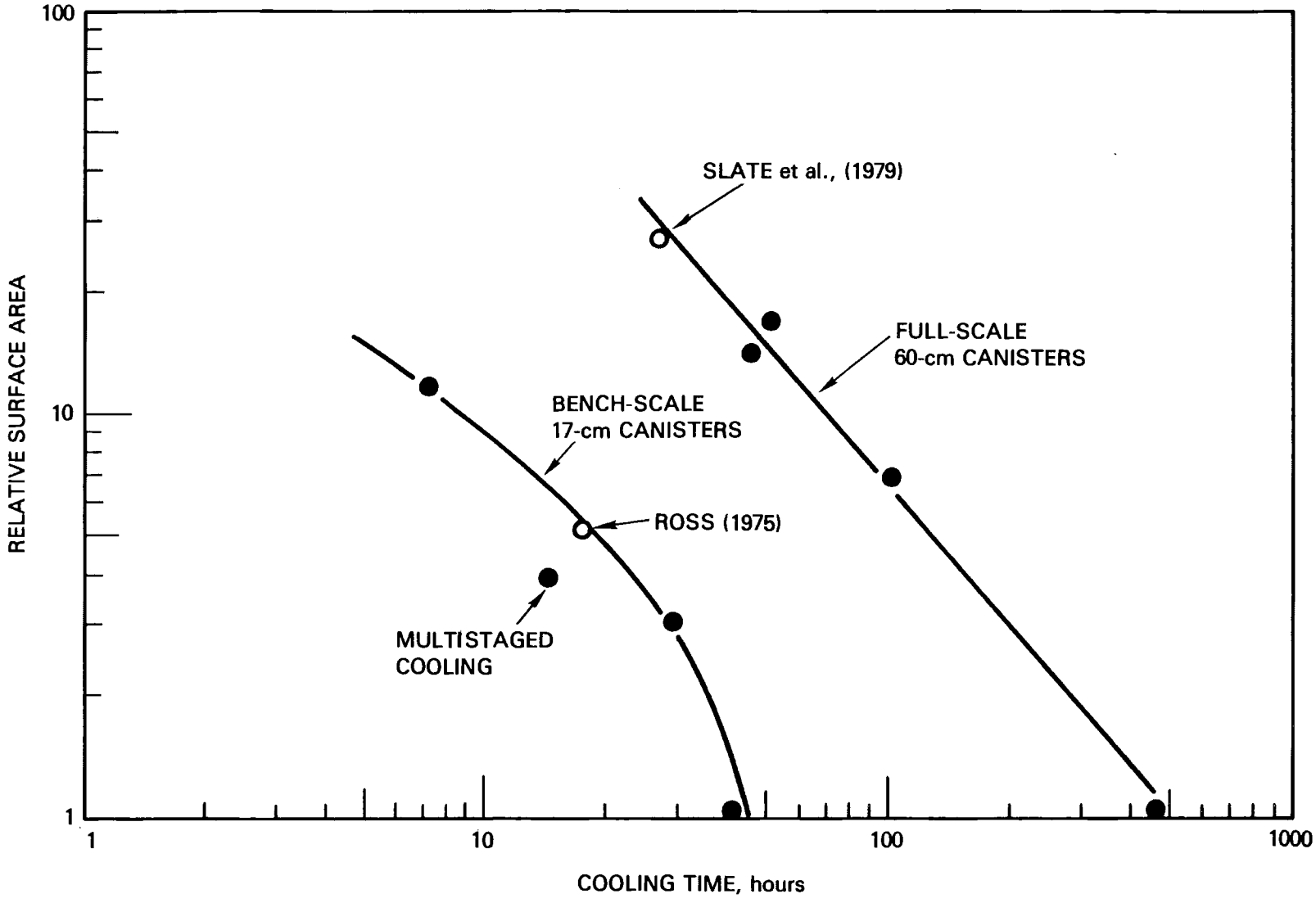

FIGURE 15. Effect of Cooling Time on Relative Surface Area of Thermal Cracks in 17-cm- and 60-cm-dia Canisters

Canister 2, thermal stresses clearly overcame the strength of the glass. Using a ΔT value of $70^{o}C$ in Equation (1), the estimated strength of the waste glass is 34 MPa. This agrees quite well with measurements of 38 MPa on small laboratory specimens as reported by Slate et al. (1978). Although a different waste glass composition was studied, Slate et al. point out that strength is almost independent of glass composition for borosilicate waste glasses.

The stress Equation (1) is not dependent on the radius of the cylindrical sample, so that a ΔT of $70^{o}C$ is a critical value for a glass strength of 34 MPa. For a 60-cm-dia canister, the cooldown time required such that ΔT never exceeds $70^{o}C$ is estimated to be 18 to 20 days. This value is based on cooling of a cylinder at an initially uniform temperature at a variable rate that is determined by a constant heat-transfer coefficient (Newman 1936). If the heat transfer coefficient is kept constant, then the cooling rate drops off naturally due to decreasing gradients in the glass. The cooldown could theoretically be maintained constant using progressively higher film coefficients without glass quality being compromised since the initial ΔT of $70^{o}C$ could be maintained until the canister is within $100^{o}C$ or so of room temperature. Based on the initial cooling rate where a ΔT of $70^{o}C$ occurs, cooldown would then take 9 to 10 days, or about half of the passive cooldown period. Cooling can thus be speeded using a dynamic rather than passive method.

Multistaged Cooling

Another alternative to the passive, single-stage method that speeds processing is to cool in several stages. If large gradients exist while the glass is cooling through its softening point (500 to $600^{o}C$), residual stresses will develop when the canister reaches thermal equilibrium with the environment. This can lead to fracturing (Slate et al. 1978). Thus, it is important to reduce radial gradients while the glass is still above softening temperatures. Conceivably, cooling can be speeded up without sacrificing glass integrity by rapidly cooling to near-softening temperatures, followed by slow cooling through this point, and then resumption of fast cooling. Such a multistaged cooldown was performed on Canister 4 as shown by its temperature history in Figure 16. Light insulation (0.64-cm ceramic board around the cooling pod)

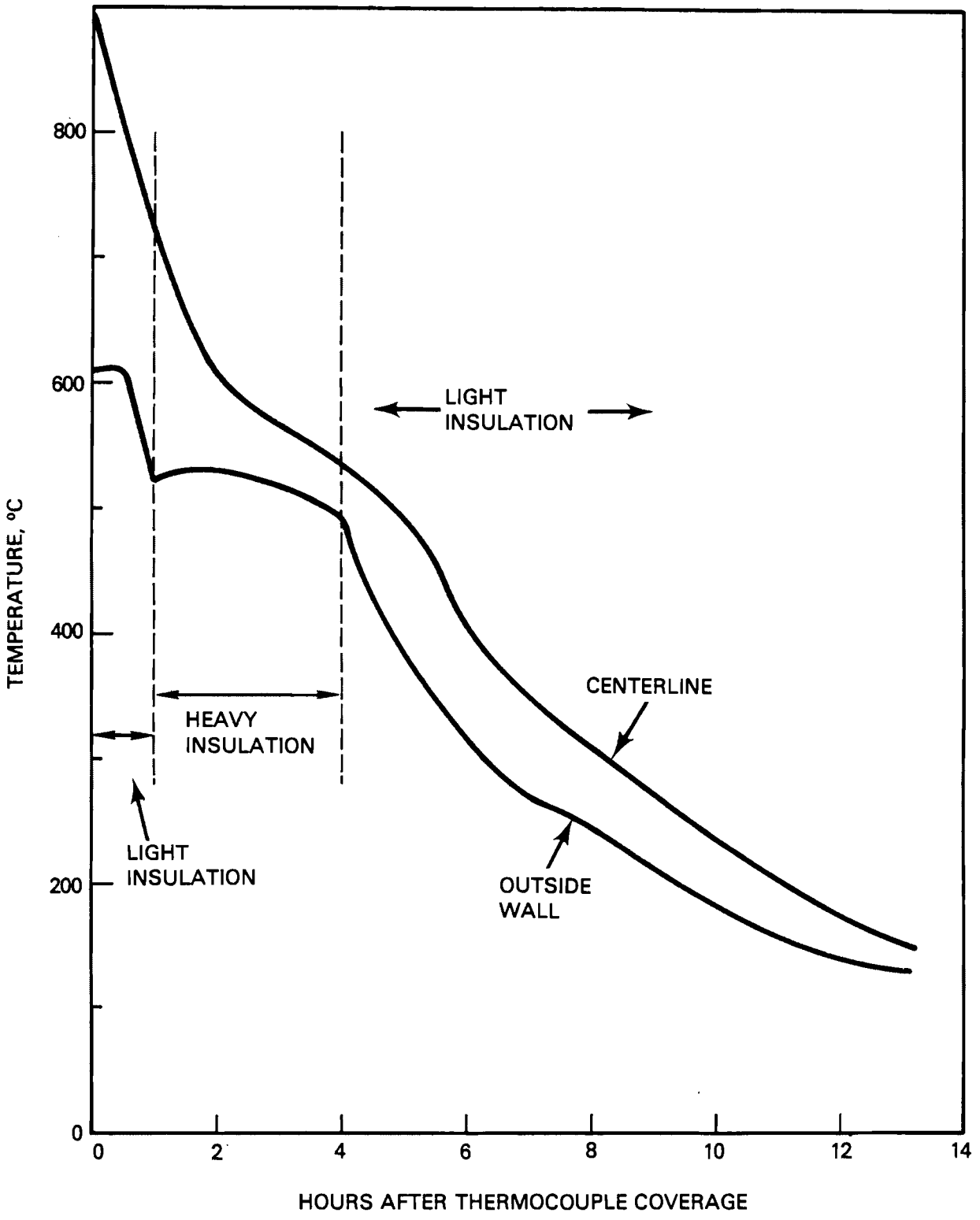

FIGURE 16. Centerline and Wall Temperatures During Multistaged Cooldown

was used for the first hour. After the canister was filled, heavy insulation (8 cm thick around the pod) was applied, thereby reducing the gradients in the canister. The centerline-to-wall temperature difference was reduced from 200°C to 40°C with the use of this heavy insulation. After 3 h, the heavy insulation was removed and fast cooling was resumed with light insulation, as during the filling. The centerline reached 100°C in about 15 h at the axial midpoint of the canister.

The extent of cracking in Canister 4 can be seen in Figure 14D and is slightly greater than in Canister 2 (Figure 14B) although Canister 2 took 28 h to cooldown. Figure 15 shows that the surface area-cooling time co-ordinate for the multistaged cooldown of Canister 4 is improved over the trend for the single-stage cooling.

This multistaged cooling has not been demonstrated on a full-scale canister although the concept should still apply. It is important to keep the walls above the softening point temperatures. This would be more difficult on a full-scale CM canister, particularly towards the bottom of the canister where cooling will progress significantly as a result of the long periods required for filling. Additional insulation on the bottom portions of the canister may be needed during filling.

The multistaged approach is more complicated than the passive approach but takes up less space due to shorter cooling times. The canister must either be transferred quickly to different insulating overpacks, or a single package must be used that will provide varying degrees of insulation using forced air or movable layers of insulation. The operating costs of such a system in a hot cell may be considerable.

GLASS/METAL INTERACTION

Cracking due to glass/metal interaction was discussed earlier for full-scale ICM canisters. This problem is not as severe in full-scale CM canisters made with carbon steel. However, the problem may exist in CM canisters made of stainless steel. In radial cross-sections of stainless steel bench-scale canisters, the glass seems to be intact. However, when a wall section of

Canister 1 (made of 304L stainless steel) was removed by sawing, the underlying glass was fractured into 3- to 4-mm-wide x 15- to 30-mm-long splinters. (A determination was made that sawing did not cause this damage when a section from the same canister was removed by electrolytic dissolution. Similar splintering was observed, although the glass had undergone appreciable attack from the phosphoric acid electropolishing solution.) Splinters of glass were bonded to the removed canister section. It was, therefore, decided to reduce or eliminate bonding by using a mold release agent, such as graphite on the inside of the canister wall.

Canister 5 was filled and cooled exactly as Canister 1, but prior to filling with glass the lower half of the canister was coated with a graphite paste (water/ethanol base). A wall section was then removed, which exposed both coated and uncoated regions. As Figure 17 indicates, the condition of underlying glass was greatly improved using graphite. The glass surface was smooth over the coated section. Also, no bonding occurred where graphite was applied; bonding did occur without the coating.

There was some concern about the stability of graphite under the temperature conditions of a full-scale CM canister-filling process since graphite can react with air. A graphite residue from the paste was found to remain adhered to a piece of stainless steel at 500°C for 18 h. This conservatively simulates the conditions during filling of a full-scale canister so that graphite should be feasible in this application. Once covered by molten glass, graphite will not react with glass at canister process temperatures. Previous experiments at Pacific Northwest Laboratory have shown that graphite reacts in air at the ICM process temperatures; therefore, it is not feasible as an ICM canister coating.

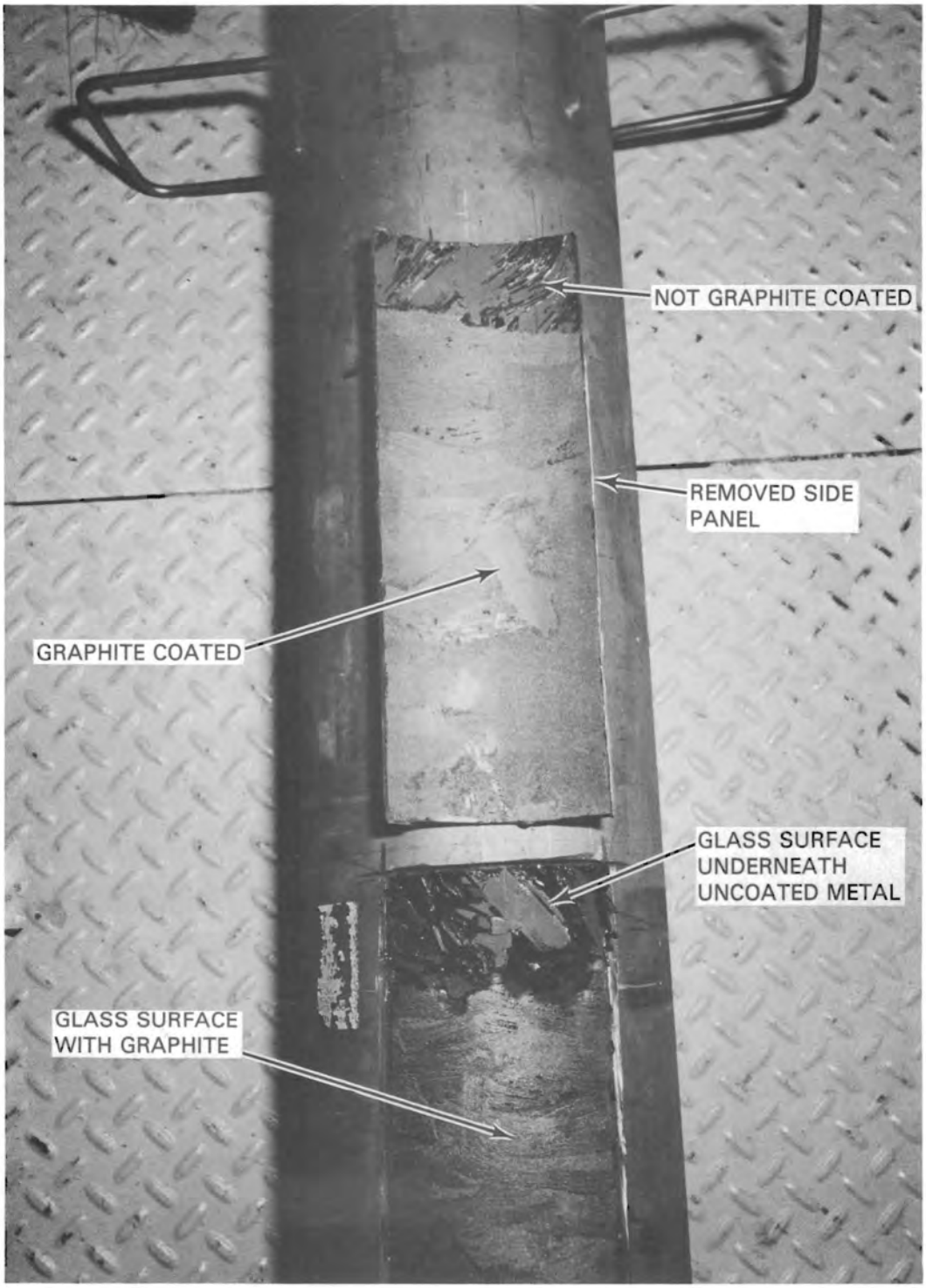

FIGURE 17. Opened Wall Section of Stainless Steel Canister Showing Effect of Graphite Coating on Glass Damage

REFERENCES

Bunnell, L. R. 1979. "Thermal and Mechanical Shock." In Annual Report on the Development and Characterization of Solidified Forms for High-Level Wastes. PNL-3060, W. A. Ross and J. E. Mendel, eds., Pacific Northwest Laboratory, Richland, Washington, pp. 63-67.

Chapman, C. C. et al. 1979. Vitrification of Hanford Wastes in a Joule-Heated Ceramic Melter and Evaluation of Resultant Canisterized Product. PNL-2904, Pacific Northwest Laboratory, Richland, Washington.

Dierks, R. D. et al. 1980. Investigation of Corrosion Experienced in a Spray Calciner/Ceramic Melter Vitrification System. PNL-3406, Pacific Northwest Laboratory, Richland, Washington.

Ethridge, E. C., D. E. Clark and L. L. Hench. 1979. "Effects of Glass Surface Area to Solution Volume Ratio on Glass Corrosion." Phys. Chem Glasses. 20:35-40.

Mecham, W. J., L. J. Jardine, R. H. Pelto, and M. J. Steindler. 1980. "Characterization of Impact Fracture of Brittle Solid Waste Forms." In Scientific Basis for Nuclear Waste Management. 2:307-314, C.J.M. Northrup, Jr., ed., Plenum Press, New York.

Newman, A. B. 1936. "Heating and Cooling Rectangular and Cylindrical Solids." Ind. and Engr. Chemistry. 28:545-548.

Perez, J. M. and J. H. Westsik, Jr. 1980. "Effects of Cracks on Glass-Leaching." ORNL Conference on the Leachability of Radioactive Solids, Gatlinburg, Tennessee, December 9-12.

Pincus, A. G. and T. R. Holmes. 1977. Annealing and Strengthening in the Glass Industry. Magazine for Industry, Inc., New York, page 23.

Ross, W. A. 1975. Quarterly Progress Report. BNWL-1893, Pacific Northwest Laboratory, Richland, Washington, pp. 35-38.

Simonen, F. A. and S. C. Slate. 1979. Stress Analysis of High-Level Waste Canisters: Methods Applications and Design Data. PNL-3036, Pacific Northwest Laboratory, Richland, Washington.

Slate, S. C. et al. 1978. "Stresses and Cracking in High Level Waste Glass." Presented at the Nuclear Regulatory Commission Conference, Denver, Colorado, December 1978.

Smith, T. H. and W. A. Ross. 1975. Impact Testing of Vitreous Simulated High Level Waste in Canisters. BNWL-1903, Pacific Northwest Laboratory, Richland, Washington.

Smith, P. K. and J. R. Wiley. 1981. "Thermal Fracturing in Glass Waste Forms." In the Proceedings of the American Ceramic Society Meeting, Bedford, Pennsylvania, October 1980.

Westsik, J. H., Jr. et al. 1978. "Leaching Studies." In Annual Report on the Development and Characterization of Solidified Forms for High-Level Wastes. PNL-3060, W. A. Ross and J. E. Mendel, eds., Pacific Northwest Laboratory, Richland, Washington, pp. 35-50.

APPENDIX A

SHEAR STRESSES AND BONDING AT INTERFACE

SHEAR STRESSES AND BONDING AT THE GLASS/CANISTER INTERFACE

In examination of canisters of simulated waste glass at PNL, an outside surface region of extensive cracking is characteristically noted. From observations of slow-cooled canisters filled by in-can melting, it appears that such cracking occurs even for very slow cooling rates. The proposed cause of this cracking has been high stress that develops during cooling as a result of the coefficient of thermal expansion mismatch between the glass and canister. In particular, the glass and canister are strongly bonded, and the differential contractions in length between the canister and glass during cooling result in severe shearing-type stresses at the glass-canister interface.

Calculated levels of stress in the region of the glass-canister interface have been reported previously. Stress levels have been calculated for specific glass and canister properties (elastic modulii and thermal expansion coefficients), and cooling temperatures and interface conditions (bonding and sliding with various coefficients of friction). The results clearly show that cooling of a canister of glass to room temperature results in glass stresses that are well in excess of the tensile and shear strengths of the glass. In recent work, finite-element calculations have been extended to predict the extent of glass cracking that occurs as a result of the high cooling stress levels.

GLASS CRACKING MODEL

Figure A.1 shows the finite-element model used for the predictions of glass-cracking patterns. The mesh represents the top portion of a 60-cm-dia canister where predicted stresses at the glass-canister interface are the greatest. The canister material was assumed to be 304L stainless steel. Stresses and cracking were the result of slow cooling of the canister of glass from temperatures above the glass softening point (assumed to be 575^{o}F). The following input parameters were selected:

- Canister wall thickness = 1.3 cm
- Canister inside dia = 60 cm

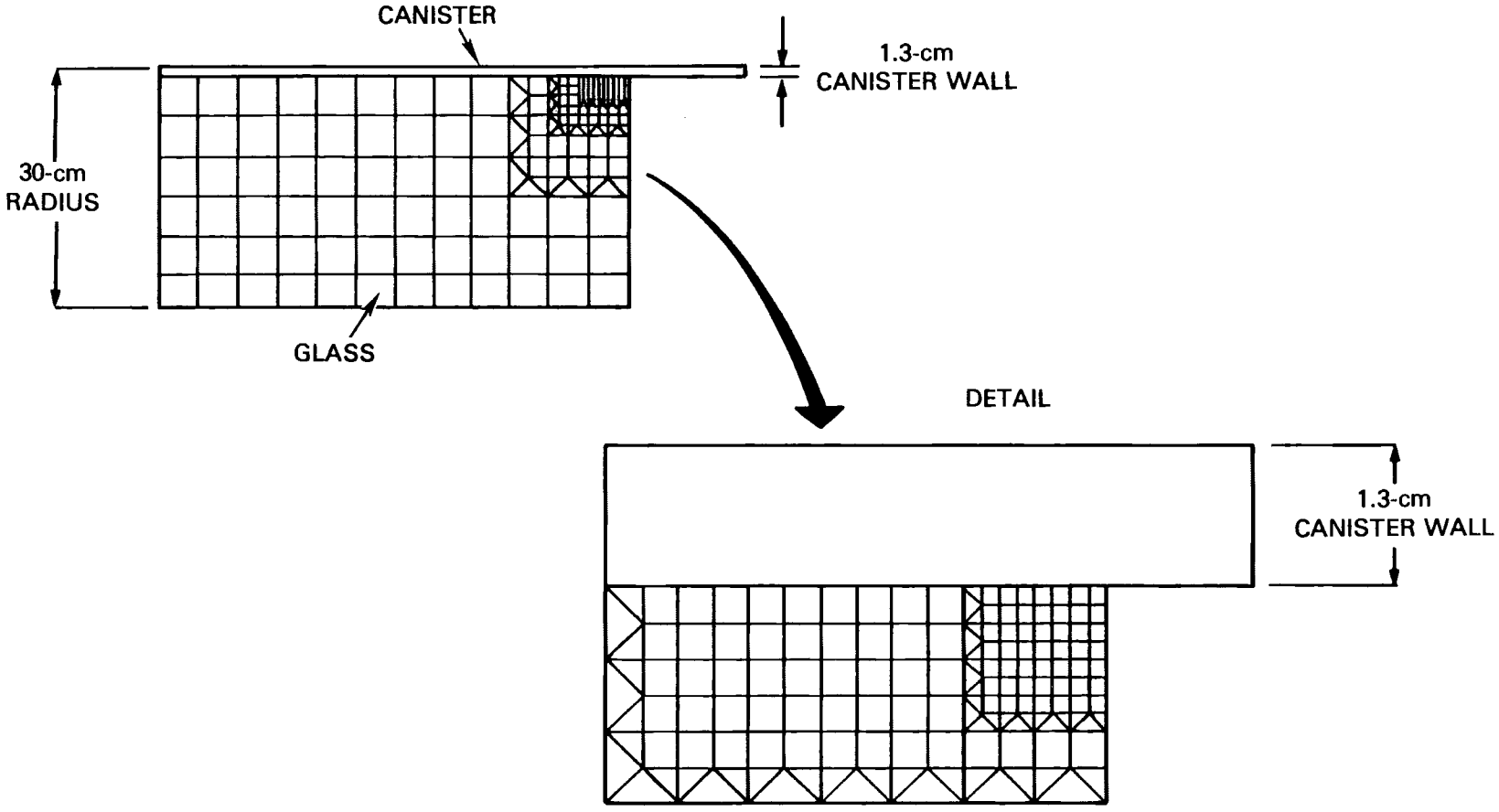

FIGURE A.1. Finite-Element Model of Glass-Canister System

- Cooling range = 575°F to Room Temperature
- Expansion coefficient of glass = $9.0 \times 10^{-6}/^{o}C$
- Expansion coefficient of canister = $17.0 \times 10^{-6}/^{o}C$
- Elastic modulus of glass = 7.6×10^{6} MPa
- Elastic modulus of canister = 1.93×10^{6} MPa
- Shear strength of glass = 200 MPa
- Implied compressive strength of glass = 400 MPa.

The elements of the mesh shown in Figure A.1 were allowed to "crack" individually once the shear stress exceeded the threshold level of 200 MPa. In cracking, the elements were assumed to fragment so that they could no longer support shear stresses. However, the fractured elements were allowed to support bulk compression stresses (i.e., hydrostatic pressure). In the calculations, the elastic constants of the fractured elements were assigned as follows:

$$\text{Shear Modulus} = G = G' \rightarrow 0$$

$$\text{Poisson's Ratio} = \nu = \nu' = 0.5 \left[\frac{E_o/(1 - 2\nu_o) - 2G'}{G' + E_o/(1 - 2\nu_o)} \right]$$

$$\text{Elastic Modulus} = E = E' = 2G'(1 + \nu'),$$

where E_o and ν_o are the elastic modulus and Poisson's ratio for the uncracked glass.

A tensile cracking model was also evaluated, but predictions of cracking using this model proved to be unsatisfactory. It was assumed that each element cracked on the plane of maximum tensile stress at a prescribed threshold (the tensile strength of the glass). After cracking, stresses could be carried parallel to the direction of cracking, and this feature of the model proved to be unacceptable. Refinement of the tensile cracking model to allow complete stress relief through secondary cracking was beyond the scope of the present effort. Instead, the simplified shear-cracking model as described above was adopted.

PREDICTED GLASS CRACKING

Figure A.2 shows predicted crack patterns along the glass-canister interface. Cracking has been indicated by computer graphics with a crack-like symbol drawn parallel to the canister wall at the centroid of each cracked element.

Cracking starts at the top outside corner of the glass, which is the location of maximum shear stresses. In the computer simulation, the cracked region advanced stepwise as the shear stress in successive elements exceeded the threshold level of 200 MPa. As the local peak in the shear stress was relieved through cracking, the shear stress peak simply advanced down the interface to a new location with each step in the cracking. Cracking then occurred at the new location. This process of repeated cracking is thought to explain how, in practice, glass becomes cracked along the entire length of the canister.

At step 10 of Figure A.2, the progress of cracking came to be arrested in the computer simulation. At this point, the predicted cracking could not extend into the coarse mesh region of Figure A.1 (the element dimensions were greater than the canister wall thickness). In the coarse mesh, the numerical stress solution could not represent the high local shear stresses. However, it can be safely concluded that with sufficient mesh refinement, the computer simulation would predict cracking along the entire length of the canister. The cost of such a full-scale computer calculation with a fully refined mesh would be prohibitive.

CONCLUSIONS

A stress-analysis model has been developed that predicts glass cracking near the glass-canister interface to a depth of somewhat less than the thickness of the canister wall. The predicted cracking is in good qualitative agreement with the cracking observed in experimental canisters.

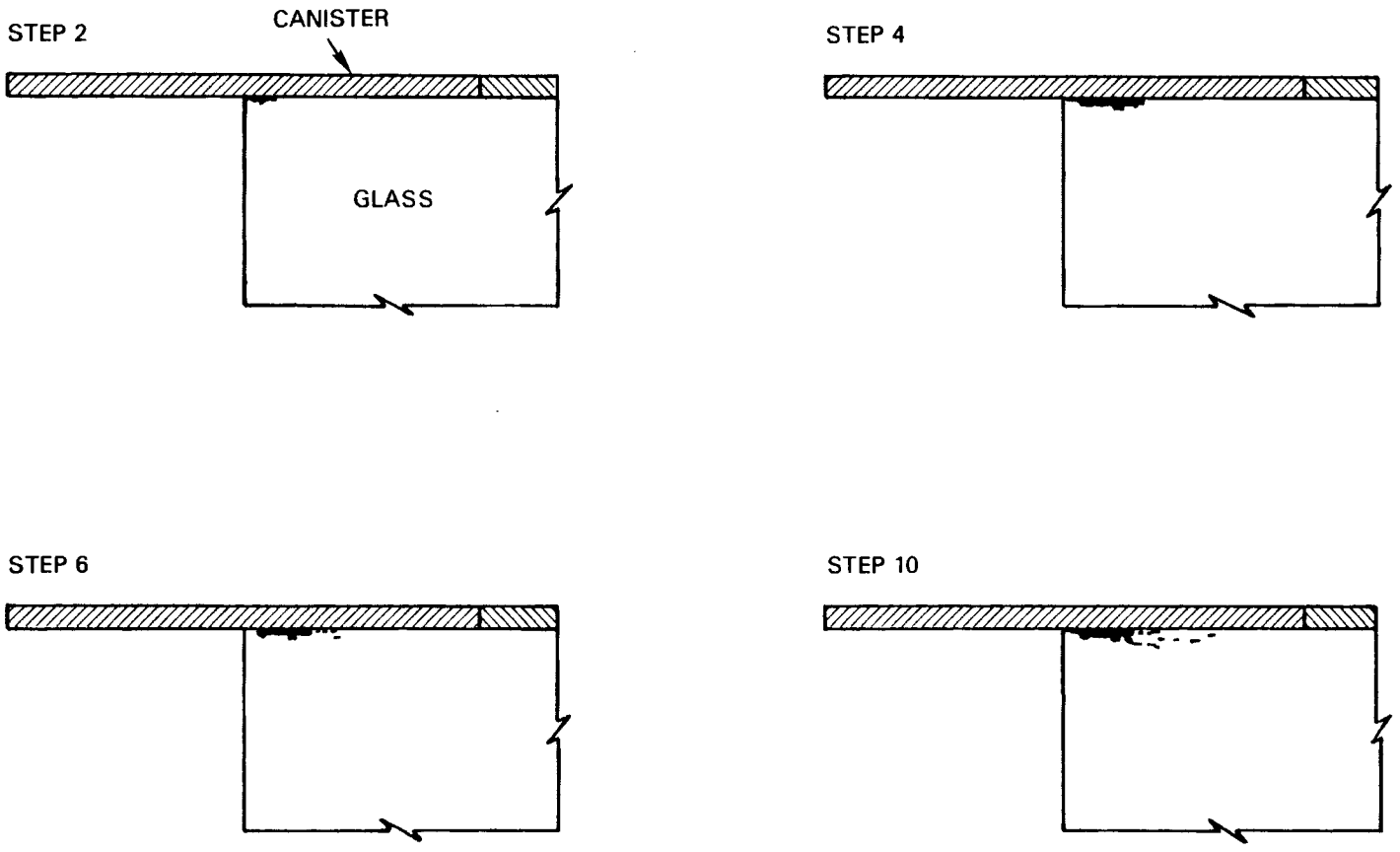

FIGURE A.2. Predicted Outside Surface Cracking in Glass of 60-cm-dia Canister

The calculations show that stresses resulting from differential thermal contractions in length between the glass and canister are probably a major cause of glass cracking in the region near the canister wall. This cracking could be reduced with a better match between the glass and canister thermal expansion coefficients, and by eliminating bonding of the glass to the canister wall.

APPENDIX B

RESIDUAL STRESSES DUE TO A PARABOLIC TEMPERATURE PROFILE IN A CYLINDER

RESIDUAL STRESSES DUE TO A PARABOLIC TEMPERATURE PROFILE IN A CYLINDER

Stresses in a cylinder are related to temperature distribution according to the following equations found in Timoshenko (1951):

$$\sigma_r = \beta\left(\frac{1}{b^2}\int_o^b Tr\,dr - \frac{1}{r^2}\int_o^r Tr\,dr\right)$$

$$\sigma_\theta = \beta\left(\frac{1}{b^2}\int_o^b Tr\,dr + \frac{1}{r^2}\int_o^r Tr\,dr - T\right)$$

$$\sigma_z = \beta\left(\frac{2}{b^2}\int_o^b Tr\,dr - T\right) ,$$

where σ is stress in three directions; r is radial position; b is radius; and T is the temperature distribution. The coefficient β is the grouping $\alpha E/(1 - \nu)$ where α is thermal expansion; E is Young's modulus; and ν is Poisson's ratio. For a parabolic temperature profile:

$$T = T_w + (T_{C_L} - T_w)\left(1 - \frac{r^2}{b^2}\right) ,$$

where T_w is the wall temperature and $T_{\text{℄}}$ is the centerline temperature. Insertion of this into the stress equations results in a relation between stress and the centerline to wall temperature drop, ΔT. The largest stress is found to be in the θ-direction (hoop stress). It is given by

$$\sigma_\theta = \frac{1}{2}\frac{\alpha E \Delta T}{1 - \nu} .$$

REFERENCE

Timoshenko, S. and J. N. Goodier. 1951. Theory of Elasticity. 2nd Edition, McGraw-Hill, New York, New York.

DISTRIBUTION

No. of Copies

OFFSITE

A. A. Churm
DOE Chicago Patent Group
9800 South Cass Avenue
Argonne, IL 60439

2 R. Y. Lowrey
DOE Albuquerque Operations Office
P.O. Box 5400
Albuquerque, NM 87185

A. L. Taboas
DOE Albuquerque Operations Office
P.O. Box 5400
Albuquerque, NM 87185

S. A. Mann
DOE Chicago Operations and Region Office
Argonne, IL 60439

J. O. Neff
Department of Energy
Columbus Program Office
505 King Avenue
Columbus, OH 43201

W. E. Mott
DOE Division of Environmental Control Technology
Washington, DC 20545

J. P. Hamric
DOE Idaho Operations Office
550 2nd St.
Idaho Falls, ID 83401

No. of Copies

J. B. Whitsett
DOE Idaho Operations Office
550 2nd St.
Idaho Falls, ID 83401

C. R. Cooley
DOE Nuclear Waste Management Programs
NE-331, GTN
Washington, DC 20545

G. H. Daly
DOE Nuclear Waste Management Programs
NE-322, GTN
Washington, DC 20545

J. E. Dieckhoner
DOE Nuclear Waste Management Programs
NE-321, GTN
Washington, DC 20545

C. H. George
DOE Nuclear Waste Management Programs
NE-330, GTN
Washington, DC 20545

C. A. Heath
DOE Nuclear Waste Management Programs
NE-330, GTN
Washington, DC 20545

M. L. Lawrence
DOE Nuclear Waste Management Programs
NE-340, GTN
Washington, DC 20545

No. of
Copies

D. J. McGoff
DOE Nuclear Waste Management
Programs
NE-320, GTN
Washington, DC 20545

S. Meyers/R. Romatowski
DOE Nuclear Waste Management
Programs
NE-30, GTN
Washington, DC 20545

G. Oertel
DOE Nuclear Waste Management
Programs
NE-320, GTN
Washington, DC 20545

A. F. Perge
DOE Nuclear Waste Management
Programs
NE-30, GTN
Washington, DC 20545

R. W. Ramsey, Jr.
DOE Nuclear Waste Management
Programs
NE-301, GTN
Washington, DC 20545

R. Romatowski
DOE Nuclear Waste Management
Programs
NE-30, GTN
Washington, DC 20545

V. Trice
DOE Nuclear Waste Management
Program
NE-30, GTN
Washington, DC 20545

D. L. Vieth
DOE Nuclear Waste Management
Programs
NE-332, GTN
Washington, DC 20545

No. of
Copies

2 S. W. Ahrends
DOE Oak Ridge Operations Office
P.O. Box E
Oak Ridge, TN 37830

D. E. Large
DOE Oak Ridge Operations Office
P.O. Box E
Oak Ridge, TN 37830

S. G. Harbinson
DOE San Francisco Operations
Office
1333 Broadway
Oakland, CA 94612

W. B. Wilson
DOE Savannah River Operations
Office
P.O. Box A
Aiken, SC 29801

R. P. Whitfield
DOE Savannah River Operations
Office
P.O. Box A
Aiken, SC 29801

J. B. Martin
Division of Waste Management
Nuclear Regulatory Commission
Washington, DC 20555

D. B. Rohrer
Division of Waste Management
Nuclear Regulatory Commission
Washington, DC 20555

R. D. Smith
Division of Waste Management
Nuclear Regulatory Commission
Washington, DC 20555

No. of Copies

R. E. Cunningham
Office of Nuclear Safety
Materials and Safeguards
Nuclear Regulatory Commission
Room 562, 7915 Eastern Avenue
Silver Springs, MD 20910

27 DOE Technical Information Center

J. A. Buckham
Allied-General Nuclear Services
P.O. Box 847
Barnwell, SC 29812

A. Williams
Allied-General Nuclear Services
P.O. Box 847
Barnwell, SC 29812

J. H. Kittel
Argonne National Laboratory
Office of Waste Management
Programs
9700 South Cass Avenue
Argonne, IL 60439

M. J. Steindler/L. E. Trevorrow
Argonne National Laboratory
9700 South Cass Avenue
Argonne, IL 60439

W. Carbiener
Battelle Memorial Institute
Office of Nuclear Waste
Isolation
505 King Avenue
Columbus, OH 43201

Beverly Rawles
Battelle Memorial Institute
Office of Nuclear Waste
Isolation
505 King Avenue
Columbus, OH 43201

No. of Copies

Research Library
Battelle Memorial Institute
505 King Avenue
Columbus, OH 43201

R. Maher, Program Manager
Waste Management Programs
Savannah River Plant
E. I. Du Pont de Nemours & Co.
Aiken, SC 29801

M. D. Boersma
E. I. Du Pont de Nemours & Co.
Savannah River Laboratory
Aiken, SC 29801

D. E. Gordon
E. I. Du Pont de Nemours & Co.
Savannah River Laboratory
Aiken, SC 29801

D. L. McIntosh
E. I. Du Pont de Nemours & Co.
Savannah River Laboratory
Aiken, SC 29801

A. L. Ayers
EG & G Idaho
P.O. Box 1625
Idaho Falls, ID 83415

R. Williams
Electric Power Research
Institute
3412 Hillview Avenue
Palo Alto, CA 94304

J. L. Larocca, Chairman
Engineering Research and
Development Authority
Empire State Plaza
Albany, NY 12223

No. of Copies

2 Environmental Protection Agency
Technological Assessment
Division (AW-559)
Office of Radiation Programs
U.S. Environmental Protection
Agency
Washington, DC 20460

J. R. Berreth
Exxon Nuclear Idaho
P.O. Box 2800
Idaho Falls, ID 83401

G. L. Ritter
Exxon Nuclear Idaho
P.O. Box 2800
Idaho Falls, ID 83401

File Copy
Exxon Nuclear Idaho
P.O. Box 2800
Idaho Falls, ID 83401

3 J. Campbell
Lawrence Livermore Laboratory
P.O. Box 808
Livermore, CA 94550

R. Roy
202 Materials Research
Laboratory
Pennsylvania State University
University Park, PA 16802

J. P. Duckworth
Plant Manager
Nuclear Fuels Services, Inc.
P.O. Box 124
West Valley, NY 14171

R. E. Blanco
Oak Ridge National Laboratory
P.O. Box Y
Oak Ridge, TN 37830

No. of Copies

J. O. Blomeke
Oak Ridge National Laboratory
P.O. Box Y
Oak Ridge, TN 37830

3 A. L. Lotts
Oak Ridge National Laboratory
P.O. Box X
Oak Ridge, TN 37830

R. S. Lowrie
Oak Ridge National Laboratory
P.O. Box Y
Oak Ridge, TN 37830

2 A. B. Martin
Rockwell International
Energy Systems Group
8900 DeSoto Avenue
Canoga Park, CA 91304

Paul Hagen
Chemical Operations
Rockwell International
Rocky Flats Plant
P.O. Box 464
Golden, CO 80401

E. Vejvoda, Director
Chemical Operations
Rockwell International
Rocy Flats Plant
P.O. Box 464
Golden, CO 80401

R. G. Kepler
Organic and Electronic
Dept. 5810
Sandia Laboratories
Albuquerque, NM 87185

W. Weart
Sandia Laboratories
Albuquerque, NM 87185

No. of Copies

P. B. Macedo
Keane Hall
Vitreous State Laboratory
The Catholic University of America
Washington, DC 20017

R. G. Post
College of Engineering
University of Arizona
Tucson, AZ 85721

L. L. Hench
Dept. of Materials Science and Engineering
University of Florida
Gainesville, FL 32611

Dr. Hayne Palmour III
2140 Burlington Engineering Laboratories
North Carolina State University
Raleigh, NC 27607

ONSITE

4 DOE Richland Operations Office

J. J. Schreiber (2)
R. E. Gerton
H. E. Ransom

4 Rockwell Hanford Operations

I. E. Reep
D. D. Wodrich (3)

72 Pacific Northwest Laboratory

W. J. Bjorklund
H. T. Blair
W. F. Bonner
D. J. Bradley
D. W. Brite
R. A. Brouns
J. L. Buelt

No. of Copies

Pacific Northwest Laboratory (contd)

R. L. Bunnell
J. R. Carrell
J. G. Carter
L. A. Chick
T. D. Chikalla
R. D. Dierks
G. J. Exarhos
M. S. Hanson
L. K. Holton
J. H. Jarrett
D. E. Knowlton
C. A. Knox
W. L. Kuhn
L. T. Lakey
D. E. Larson
R. O. Lokken
G. B. Long (3)
J. L. McElroy
G. B. Mellinger
J. E. Mendel
R. D. Nelson
J. F. Nesbitt
R. E. Nightingale
R. D. Peters (10)
A. M. Platt
W. A. Ross
J. M. Rusin
R. J. Serne
D. H. Siemens
F. A. Simonen
S. C. Slate (10)
C. L. Timmerman
R. L. Treat
R. P. Turcotte
H. H. Van Tuyl
J. W. Wald
J. H. Westsik, Jr.
D. P. Williams
Technical Information (5)
Publishing Coordination EI (2)